Martian North Polar Crater Morphology: Implications for an Aquifer

A Senior Honor Thesis by:

Amy Lynn Bacastow

Department of Geology
Washington and Lee University
Lexington, VA 24450

May 2006

ABSTRACT

Recent studies of martian north polar craters have suggested that they have more cavity fill than the global crater population, and that the morphology of the crater fill is—in some cases—similar to pingo structures on Earth. The presence of hydraulic pingos in polar impact craters implies a polar region aquifer or, alternately, the melting of a permafrost layer upon impact. This study examines the properties and distribution of impact craters in the north polar region of mars, which contain anomalous fill patterns similar to terrestrial pingos. We use high-resolution (256 pixels/degree or about 230 meters/pixel) topographic data from the Mars Orbiter Laser Altimeter (MOLA) instrument on the Mars Global Surveyor Mission to characterize the impact craters and their cavity fill materials. We classified the polar craters into three groups: Types I, II, and III. We find that those craters (Type II and III) with anomalous central fill are shallower than other near-polar craters of similar diameter. Within 18° of the Martian North Pole, nearly all of the largest complex craters have large, central fill features. The moderate-sized complex craters have fewer anomalous fill attributes while similar fill are not found in the smaller, simple craters. Anomalous, central features are more common at high latitudes. When we model the possible polar aquifer as having a linearly increasing depth with increasing distance from the pole, we find that polar crater classification correlates strongly with the depth to aquifer. This is consistent with larger impact crater excavation reaching an aquifer and resulting in hydraulic pingo formation. We suggest that smaller crater excavation depths are not deep enough to reach the modeled aquifer and thus have no pingo-like features. However, a difference in morphology between the Type II and Type III craters suggests another process in the north polar region. Some possible explanations towards the modification of Types II or III are differential solar radiation or wind transport. However, it is possible that Type II and Type III craters are formed from two entirely different processes and not by pingo formation. We are left, then to decide whether Type II and Type III craters are formed by the same mechanism (aquifer puncture or permafrost melting) and are subsequently modified differentially or if they are formed by two independent mechanisms.

INTRODUCTION AND BACKGROUND INFORMATION

Impact craters have been a topic of intense study in the planetary world beginning in ancient times with Galileo's "Sidereus Nuncius" ("The Starry Messenger") published in 1610, which discussed the origin of lunar craters. In 1906, a great advance for crater studies was made when D.M. Barringer proved that Meteor Crater in Arizona was formed by a meteorite impact. Further advancements were made on the heels of WWII when concerns arose regarding the physical impact of explosion craters (Melosh, 1989, p3). Since then, the field of impact craters has grown in leaps and bounds and has yielded data on ejecta properties, deformation of the surface, age of the surface, crater morphology, and more.

Following the Viking mission to Mars in the 1970s, scientists analyzed satellite images and gained an incredible amount of knowledge regarding Martian impact craters. Continuing studies make use of the Viking data including those on crater-size frequency distribution (Werner, 2005), calculating ejecta volume (Ackerman, 2005), and examining possible former lakes in craters (Cabrol, 1999). From Viking images, Dr. Nadine Barlow created the *Catalog of Large Martian Impact Craters* in the 1980s, which was then revised using Mars Global Surveyor and Mars Odyssey data; this catalog contains information on more than 42,000 impact craters on Mars (Barlow, 2005). Although useful, this study does not rely on Barlow's catalog, but attempts to make a similar, independent catalog of north polar impact craters on Mars based on their morphology and, in particular, their central features.

Impact craters are divided into several categories based on morphology; two of these divisions are "simple" and "complex" craters. The planetary community classifies simple craters as those less than 7 km in diameter from rim to rim; these craters are "bowl-shaped" in form. Meteor Crater in Arizona is an excellent example of this morphology. Larger than 7 km in diameter from rim to rim, complex craters often have wall terraces, central peaks, and flat floors unlike simple craters which typically have a rounded-out bottom. A central peak (Figure 1) forms when the initial shockwave propagated from the impact rebounds back to the center (Melosh, 1989, p14-18). An analogy for this process is dropping a pebble into a pool of water and watching the small peak form in the center when the wave rebounds (Figure 2). Some craters larger than 7 km do not have a central peak either due to deposition and/or erosion or because they fall into a separate category such as those with double layer ejecta. Central peaks in complex craters play an important role in this study with regard to categorizing craters based on central feature morphology.

Figure 1: Cross-sectional profile of a complex crater showing the central peak in the middle.

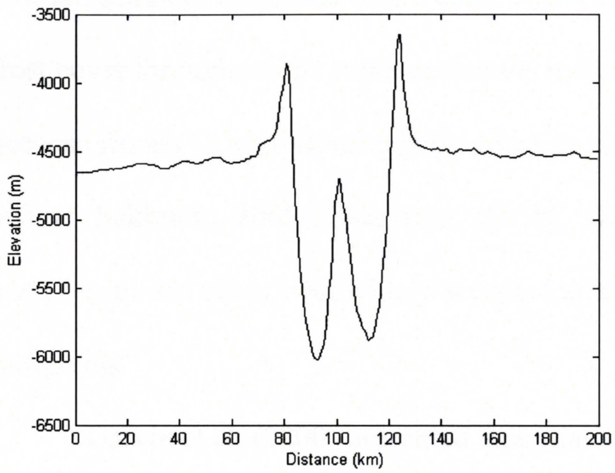

Figure 2: A peak forms in water when a pebble is dropped into it; this is analogous to the forming of a central peak in complex craters.

http://www.sciences-po.org/projets_collectifs/eau/home.htm

Many studies have focused on the complexities of Martian impact craters. Cabrol et al. (1997) conducted a study of frost mounds in Gusev crater in the southern hemisphere of Mars and discovered some features that are similar in morphology to terrestrial pingos.

> "The pressure and heat during an impact event generate a layer of melt material that can be considered as impermeable... [The impact] formed another layer of melt material generating a natural lock that confined locally the water circulating underground... On Earth, this system generates groundwater springs that tend to freeze. When a spring is closed by the formation of a pingo, the water emerges nearby..."

On earth, the growth rate for pingos is 0.01-0.34 m/yr. At this rate, a 100m high pingo would have taken 294 to 10,000 years to form (Cabrol et al., 1997).

Another set of papers lending a great deal of information as well as inspiration are by Dr. Susan Sakimoto who has conducted extensive research on Mars polar impact craters and central mounds. She hypothesizes that central mounds found in polar impact craters are analogs to terrestrial pingos as earlier proposed for some structures in the Martian southern hemisphere by Cabrol et al. (1997). These mounds preserve their bright frost cover throughout the summer months indicating that the mounds are likely water ice because frozen CO_2 sublimates in the Martian summer months leaving only the water ice behind (Sakimoto, 2005a; Sakimoto, 2005b). Cabrol and Sakimoto's hypotheses are quite recent and are not yet widely accepted among the planetary community, but are intriguing.

Garvin et al. (2000) presented an initial set of depth-diameter relationships for impact craters in three categories: simple, complex, and "large" (diameter > 100 km). This study also yielded a set of rim height-diameter relationships again based on three groups according to crater size (Garvin, et al., 2000a). Garvin et al. (200b) presented data on crater morphology, in particular those of "ice-associated" craters above 57°N (Garvin et al., 2000b). Throughout the following years, Garvin and others continued to fine tune their data analyses to produce a set of relationship equations (Garvin, et al., 2003), which are used in this study. Equations were given for predicting depth, rim height, central peak height, central peak diameter, cavity shape, cavity shape fit coefficient, cavity shape fit exponent, and inner cavity wall slope based on the global fresh crater population. This study uses only the depth and rim height equations (Table 1).

Table 1: Equations predicting crater depth and crater rim height from crater diameter based on Garvin et al. (2003), where D is crater diameter (km). **D>100 km.

Parameter	Simple Crater	Complex Crater	Large Crater **
Depth (km)	$d=0.21D^{0.81}$	$d=0.36D^{0.49}$	
Rim Height (km)	$h=0.04D^{0.31}$	$h=0.02D^{0.84}$	$h=0.12D^{0.35}$

Boyce et al., (2005) conducted a depth and diameter survey of 460 craters in Thyles Rupes and Prometheus, both of which are craters found in the southern hemisphere of Mars; these craters were compared to those found in the northern lowland plains. Upon comparison, they found that the crater populations in high latitudes are lacking in fresh craters, which may be due to the deposition of ice and dust. They concluded that the lack of fresh craters in the high latitudes may suggest "a recent degradational or burial process exclusive to the high-latitudes of Mars" (Boyce et al., 2005).

METHODS

Given these studies of terrestrial and Martian impact crater populations, the knowledge of variable morphology and process in the north polar region and the likely existence of pingos, this study focuses on complex craters with anomalous central features in place of an expected central peak in an effort to determine the origins of these features. Much of this research was conducted using satellite DEMs for morphological analysis. Data for 350 Martian north polar impact craters were gathered from high resolution (256 pixels/degree) DEMs collected by the Mars Orbiter Laser Altimeter (MOLA) on the Mars Global Surveyor which was launched in 1996 (Slaveny et al., 1996). Gridview (Roark, J.H., 2004) was used to identify different crater shapes, note crater location, determine crater volume, generate crater profiles, and measure crater depth and diameter. Crater relationships from Garvin et al. (2000b; Table 1) yielded predicted crater shapes based on global data. These data and observed morphology were used to divide crater subjects into three crater categories.

Crater Selection

Impact craters were visually identified from the DEMs with five km as the lower limit of the study due to the resolution of the DEMs. From a potential total of 559 craters only 350 met the criteria for this study. Those that did not meet the criteria were eliminated for three reasons: (1) the craters were less then 5 km in diameter and fell below the resolution of the data, (2) erosion and modification of older craters made it impossible to draw a suitable shape around the crater cavity, making volume calculation too speculative, or (3) the bottom of the crater was above the level of the pre-impact surface. Some of these latter craters likely have been filled by dust and ejecta material from surrounding impacts, and therefore are too modified to produce reliable data. Other "craters" in this second group may not be impact craters at all, but instead are volcanic calderas.

Morphological Measurements

Data used in analysis for this study come from two sources: (1) raw morphological measurements and (2) derived, predicted measurements. Derived data, though, is dependent on the raw measurements collected in Gridview. Depth I is the distance from the rim apex to the bottom of the crater, which is the depth used by Garvin et al. (2003). Crater depth below the pre-impact surface (Depth II) was also measured to eliminate the potential error produced by rim erosion. The pre-impact surface was determined by visually identifying the surface beyond the ejecta blanket of the impact crater and determining the elevation. If the surfaces beyond either end of the ejecta blanket in profile are not equal, a connecting line between the elevations was used for measurements.

Diameter was simply the distance from rim apex to rim apex. Rim height was the height of the rim apex above the pre-impact surface. Depths I and II, diameter, and rim height were obtained from crater profiles. Each crater was profiled in four directions (N-S, W-E, NW-SE, NE-SW) and the data were averaged to produce a single value for each crater characteristic. In addition to these measurements, latitude, longitude, elevation, and volume were also collected.

Derived Crater Characteristics

Derived data includes predicted depth I, predicted depth II, fraction of filled crater depth, predicted crater cavity volume, and predicted fill volume. The depth below the pre-impact surface (depth II) is derived using the rim height and depth (depth I) equations from Garvin et al. (2003), which were determined from diameter (Table 2).

Table 2: Derived equations for Depth II from Garvin et al. (2003), where D is Crater Diameter (km) **D > 100km

Parameter	Simple Crater	Complex Crater	Large Complex Crater **
Depth II (km)	$0.21D^{0.81}-0.04D^{0.31}$	$0.36D^{0.49}-0.02D^{0.84}$	$0.36D^{0.49}-0.12D^{0.35}$

The filled fraction of crater depth is computed as:

$$\frac{predicted\ depth\ I - observed\ depth\ I}{predicted\ depth\ I} \qquad \textbf{\textit{Equation 1}}$$

This measurement is intended to show the relative amount of filling for craters. Craters with a fraction close to zero are relatively fresh because their observed depth and predicted depth are nearly the same. On the other hand, those with larger fractions are not "fresh" and filling has occurred; the amount of filling increases as the fraction approaches one.

Predicted crater cavity volume and predicted volume of crater fill data were slightly more complex to calculate. The shape of the crater was determined to be roughly parabolic ($y=ax^2$) where the coefficient, ***a***, is derived. With the vertex set at (0, 0), ***a*** was derived using ***y*** as the predicted depth I, and ***x*** as the diameter/2.

$$a = \frac{y}{x^2} = \frac{predicted\ dpeth\ I}{(diameter/2)} \qquad \textbf{\textit{Equation 2}}$$

Predicted depth I was be used because the volume of the crater cavity was calculated from the top of the rim to the bottom of the crater. The parabolic equation (Figure 3) was then integrated to obtain the volume of the space within the curve as if it were revolved around the y-axis (Equation 3).

$$predicted\ volume = \int_0^{depth} \frac{\pi y}{a} \Delta y = \int_0^{depth} \frac{\pi}{a}\left[\frac{y^2}{2}\right]$$

$$predicted\ volume = \frac{\pi}{a}\left[\frac{(depth)^2}{2}\right] \qquad \textbf{\textit{Equation 3}}$$

Figure 3: Example topographic profile of an example impact crater with the calculated parabola in dashed blue.

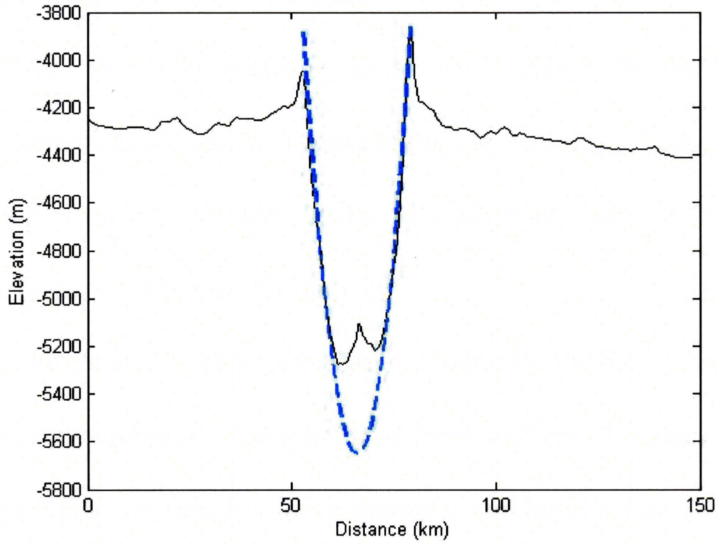

The volume of the crater cavity filled by dust, snow, or other materials was derived from the difference between the predicted and the observed volumes as follows:

$$\textit{predicted fill volume} = \textit{predicted volume} - \textit{observed volume} \qquad \textbf{\textit{Equation 4}}$$

CRATER CATEGORIZATION

Craters in this study were grouped into three separate categories (Types I, II, and III) based predominantly on central features, but specifically on characteristics such as shape, symmetry, and size.

Type I craters include both simple and some complex craters. For the complex craters, the central peaks are the only central feature to the crater. These central peaks are nearly perfectly symmetrical, occupy a very small portion of the crater floor, and do not rise above the pre-impact surface level (Figures 4A and 5A). The simple craters in this category have no central peak, so they have no central feature. Some "complex" craters may lack a central peak due to erosion and deposition.

Type II craters have a large, central feature (Figures 4B and 5B) rather than the smaller, conical central peak of Type I craters. These central features are generally symmetrical and, in contrast to central peaks of Type I, rise above the level of the pre-impact surface. The central feature of these craters is completely encircled by a moat. In addition, Type II central features are significantly larger in diameter than central peaks and occupy nearly the entire crater floor.

Type III craters are the most variable in shape (Figure 13). They have a moderately large central feature, though not as large as Type II craters (Figure 4C and 5C). These central features are smaller in diameter and height than Type II craters but larger than Type I craters. They also have a moat, but it is not continuous around the entire central feature in contrast to Type II craters. The central features appear in a wide range of asymmetrical shapes and sizes, but are consistently located on the western half of these craters.

Figure 4: Shaded relief topography of Type I (A), Type II (B), and Type III (C) craters

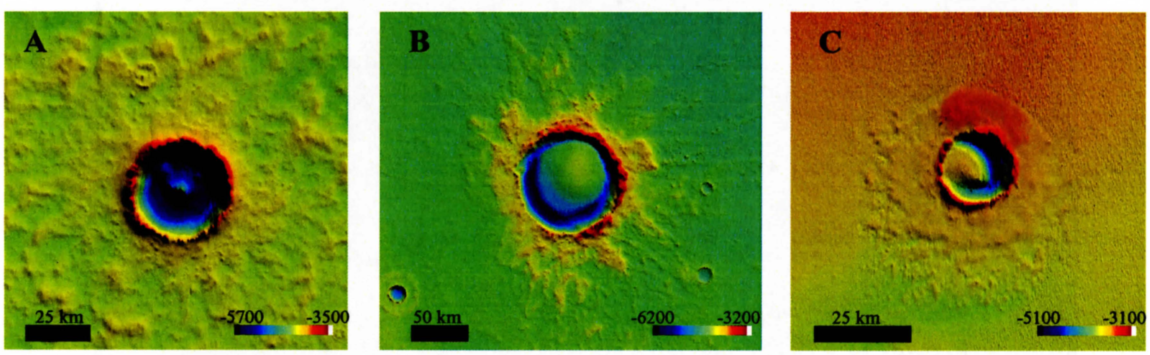

Figure 5: Cross-sections of craters shown in Figure 4.

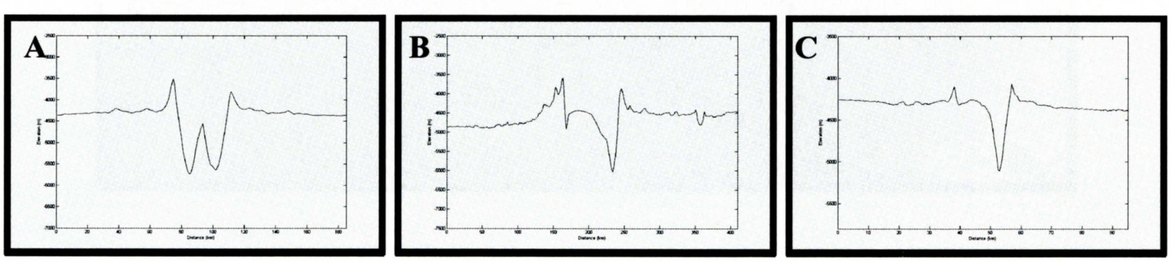

RESULTS

Crater type and crater characteristics appear to be latitude dependent. Type III craters (Figures 4C and 5C) occur in a narrow latitude band closest to the pole between 78.6 and 81.6 °N (Figure 6); craters having this morphology are not found elsewhere in the study area. Type II craters (Figures 4B and 5B) are located slightly south of Type III craters, but also in a limited latitude band; these craters are only located between 71.2 and 77.2°N. Type I craters (Figures 4A and 5A) are located throughout the study area in a range of 57.6-81.7 °N without any particular latitudinal concentration.

Figure 6: Polar plot of locations of all craters in study laid over a shaded relief DEM. Small white points are Type I craters, large white points are Type II craters, and medium white points are Type III craters.

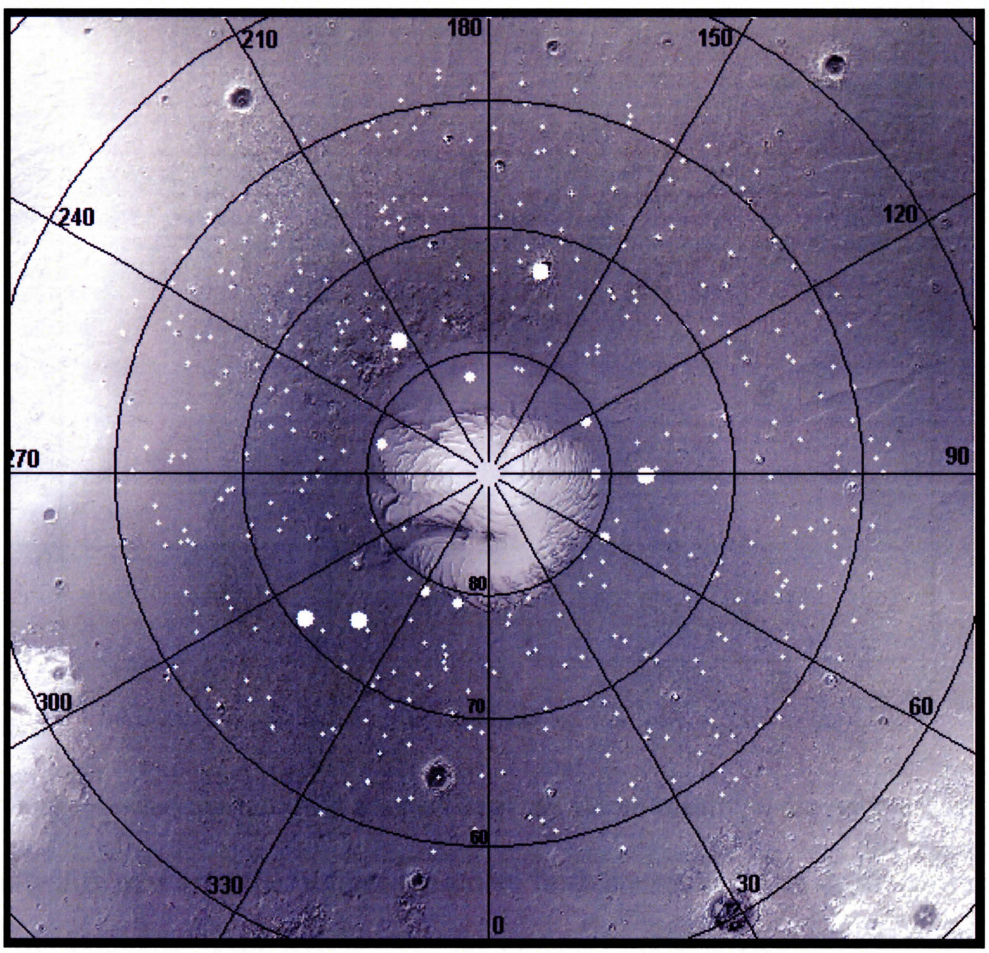

The filled fraction of crater depth (Equation 1) is also latitude dependent (Figure 7). The fraction gives a value of zero for a fresh crater and values approaching 1 for filled craters. Clearly, as latitude increases the number of fresh crater decreases. Because filled fraction values are generated by predicted data derived from global average equations, some negative values are to be expected.

Figure 7: Fraction of crater depth not filled vs. latitude. Craters with a fraction value of one are considered "fresh" with no filling. Craters with a fraction less than one exhibit some amount of filling.

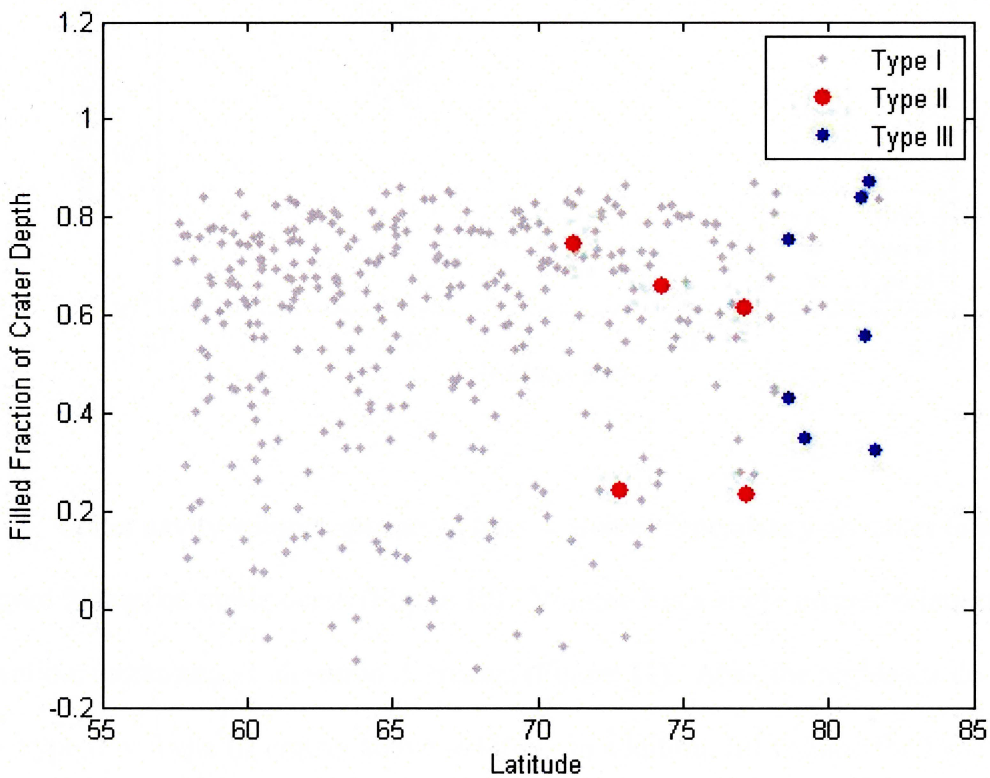

As suggested by the filled fraction of crater depth results, most polar craters are drastically different from the fit lines for global fresh craters based on depth and diameter (Figure 8). Very few of the craters lie on the fit lines (Table 2) derived from Garvin et al.

(2003). Moreover, Type II and Type III craters are shallower than craters of similar diameter. Type II craters tend to be the largest in diameter while Type III craters tend to be in a moderate diameter range and Type I craters have a wide diameter range.

Figure 8: Crater Depth II vs. Diameter. Lines are from global fit equations from Garvin et al. (2003) (Table 2).

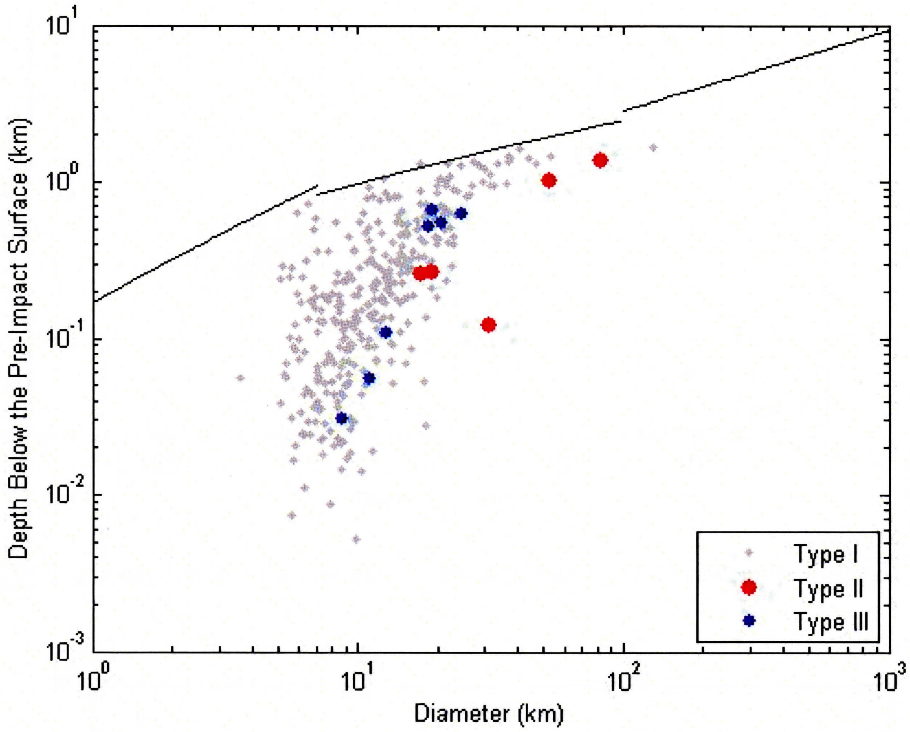

Crater cavity volume appears to have a greater dependency on crater diameter (Figure 9) than on crater depth (Figure 10). Volume has a slight inverse relationship with elevation, increasing as elevation decreases (Figure 11). Also, the highlands do not have any Type II or Type III craters above -4440m. In addition, fill volume for Type III craters is the largest and Type II fill volume is within the upper ranges of the Type I craters (Figure 12). One anomalous Type I crater has the largest volume fill, but this crater is abnormally large and has different properties than other craters in this study.

Figure 9: Observed Crater Diameter vs. Observed Crater Cavity Volume

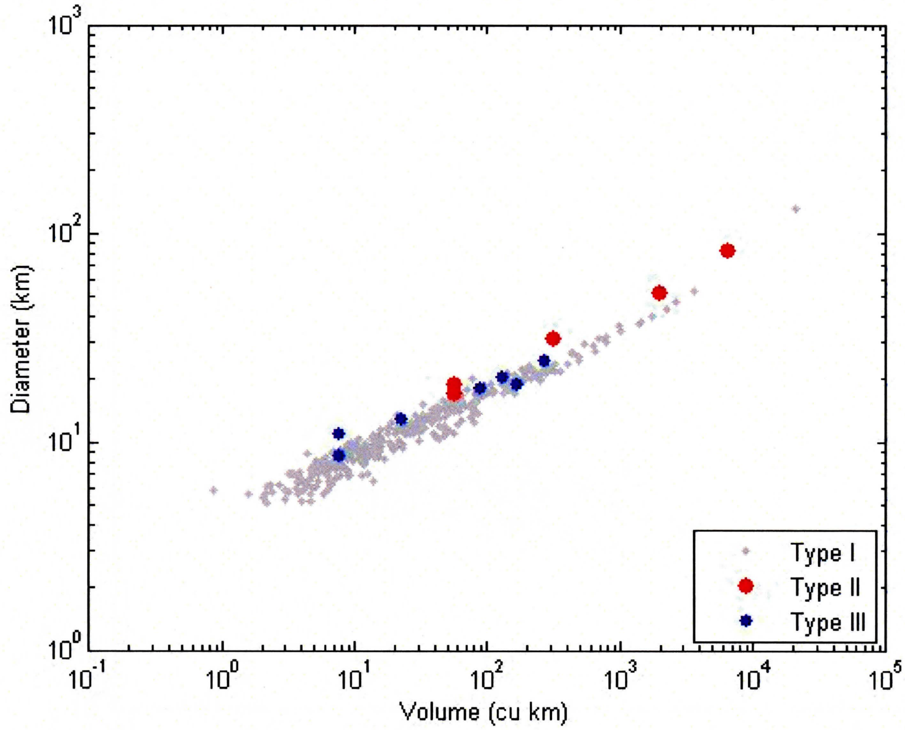

Figure 10: Crater depth below the pre-impact surface (Depth II) vs. Crater cavity Volume

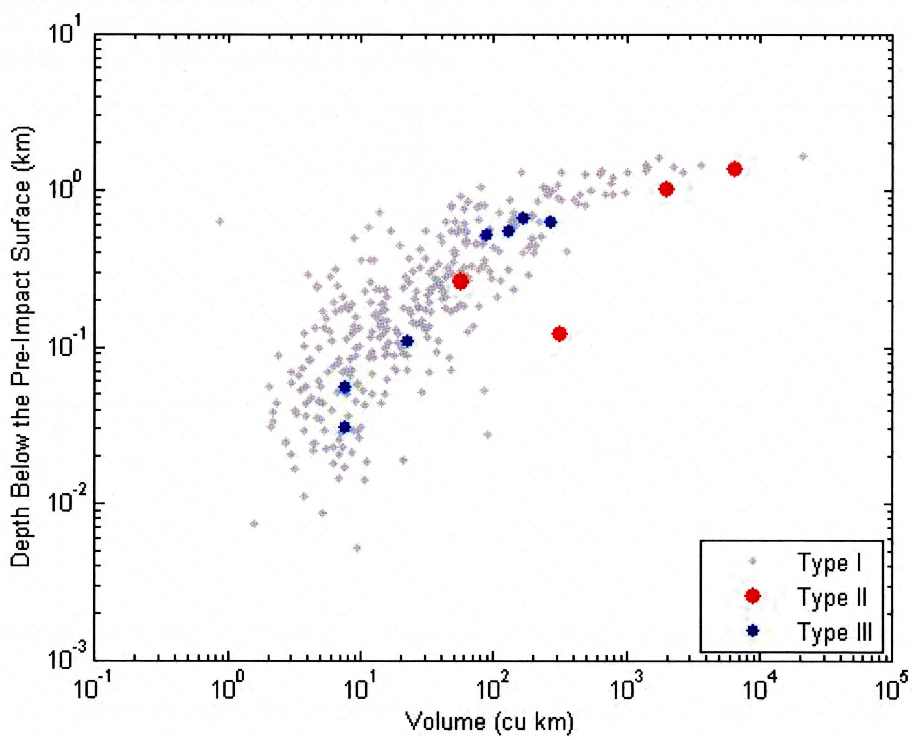

Figure 11: Crater elevation vs. crater volume. Note that Type II and Type III craters do not appear above -4400m

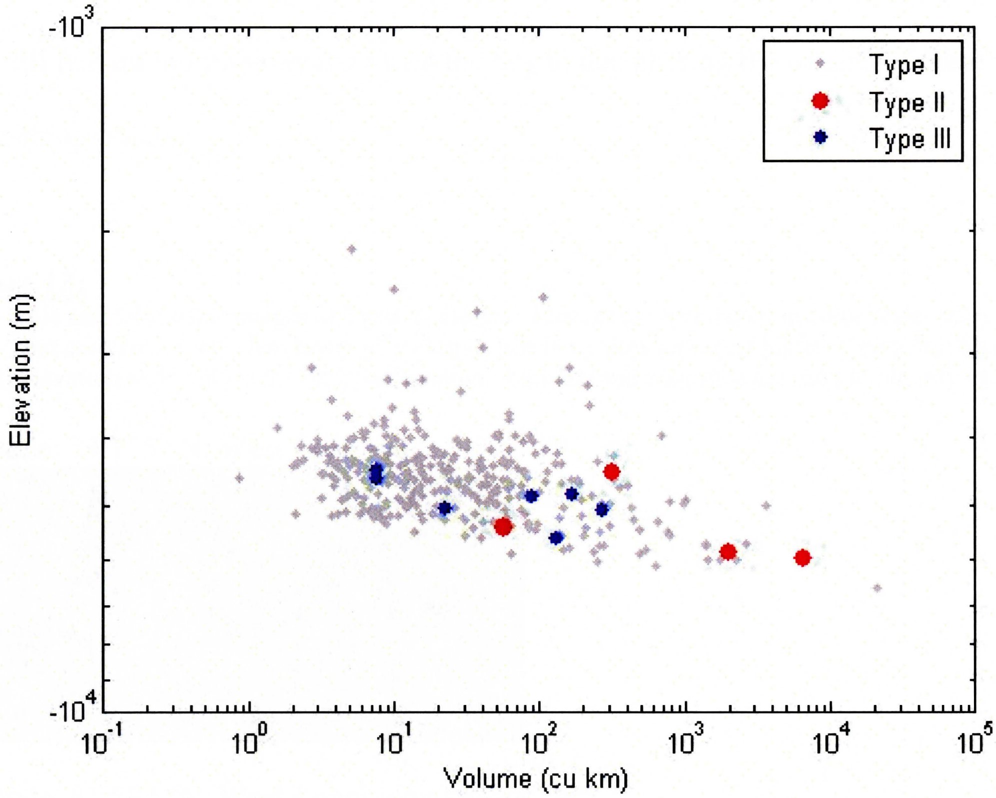

Figure 12: Crater Fill Volume vs. latitude. The plot on the left represents all the data. The plot on the right shows a zoomed-in section of the plot for easier viewing by eliminating the two largest outliers as well as negative values. Fill Volume is in cubic km.

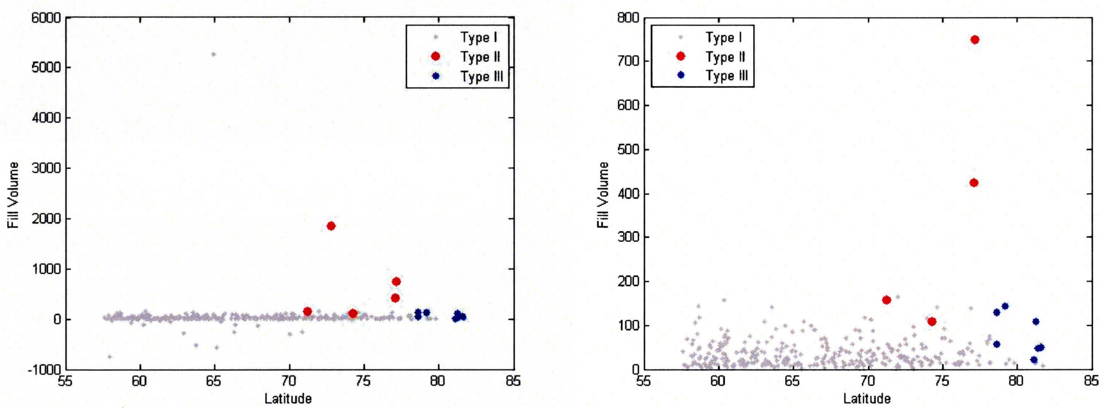

The fill in Type III crater is always located on the western section of the crater (Figure 13). This was first observed when making the initial crater categories. After further examination of the Type III craters, their morphology, and their latitude dependence, the asymmetrical nature of their fill became an important piece of analysis. This fill feature morphology may lend the key to deciphering the origins of these anomalous craters.

Figure 13:
Grey-scale and false color images of Type III craters. Elevations represented in color scales vary for each image, but cool colors represent lower elevations while hot colors represent higher elevations; black is the lowest elevation and white is the highest elevation. Latitude and longitude are used to identify each crater.

Latitude: 79.125 °N West Longitude: 299.09 °W

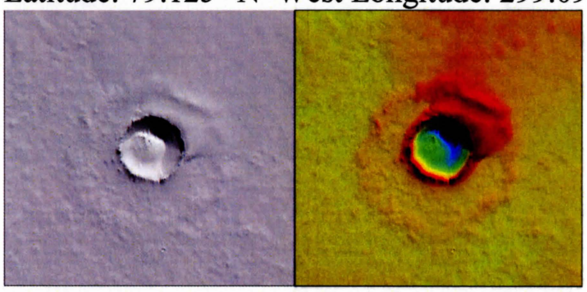

Latitude: 81.582 °N West Longitude: 169.88 °W

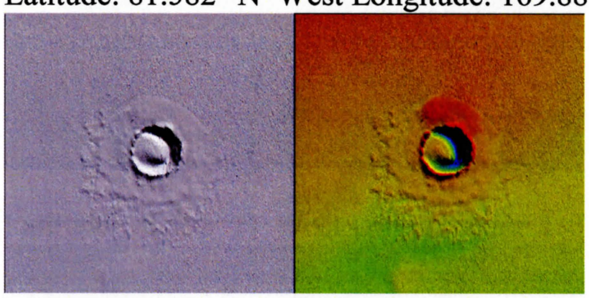

Latitude: 81.264 °N West Longitude: 105.17 °W

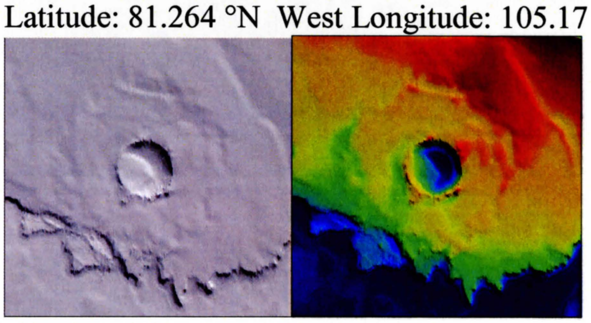

Latitude: 78.606 °N West Longitude: 13.005 °W

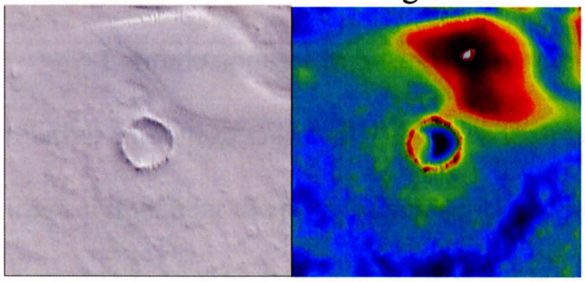

Latitude: 81.101 °N West Longitude: 271.17 °W

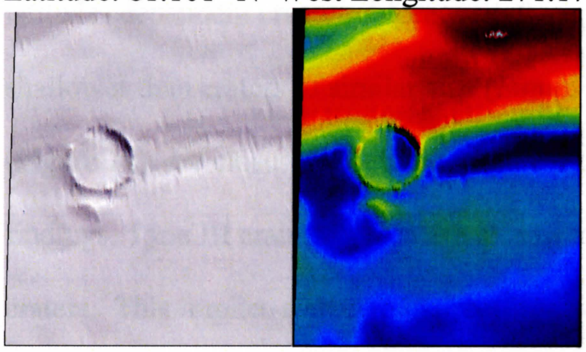

Latitude: 81.36 °N West Longitude: 242.75 °W

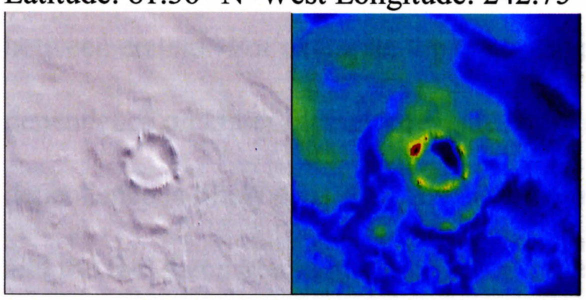

Latitude: 78.598 °N West Longitude: 28.233 °W

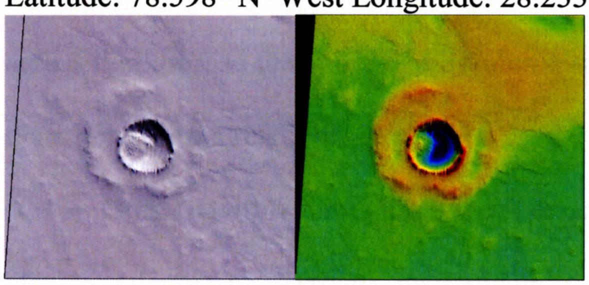

ANALYSIS

Latitude appears to be a primary role in the morphology of craters on mars. The relative amount of crater fill increases with latitude (Figure 7) leading to a decrease in fresh craters near the pole, which supports the findings of Boyce et al. (2005) that crater populations in high latitudes are lacking in fresh craters. Type II and Type III are latitude- dependent craters. Moreover, Type II and Type III craters, both of which are shallower than craters of similar size (Figure 8) and have larger amounts of fill volume (Figure 12), are closest to the pole (Figure 6). However, in contrast to these general findings, Type III craters, which are closest to the pole, have less fill volume than Type II craters. This implies a change in processes very near the pole versus the entire polar area.

This apparent filling process(es) may have an effect on other relationships between craters. For example, the crater cavity volume appears to have a much stronger dependence on crater diameter (Figure 9) than on crater depth (Figure 10). This dependence is likely caused by insubstantial modification of crater diameter over time and the fact that craters tend to be 20-50 times wider than they are deep. Crater depth, however, alters more quickly as the crater is filled. This filling is not spatially consistent across the floor, so the crater depth-volume relationship is more variable than the crater diameter-volume relationship.

Crater cavity volume has a weak dependence on elevation, increasing slightly as elevation decreases. Perhaps, geologic units at lower elevations are softer than those at higher elevations, allowing bolides to punch farther into the surface. Currently, there are planet-wide geologic maps of Mars, but few that would be detailed enough to explain this diameter-elevation relationship at this time. Another explanation could be that the lower elevations have had more filling from erosion of the highlands, thus creating a softer ground and allowing the bolide to punch in farther.

Type II and Type III craters have more fill volume, are larger in diameter, are located closer to the poles, and have anomalous central features in comparison to Type I craters. The question then is what causes these features? We first examine possible modes of filling for the craters and look at their plausibility for causing the anomalous central features. Dust should be ubiquitous over the entire planet, so it is not probable that this is the cause for the central fill. Snow is a possibility, but that should be everywhere in the polar region, so we would expect it to affect more than just these few craters. Polar Layered Deposits (Fenton and Herkenhoff, 2000) could be the cause, but the central features do not have the characteristic striping of layers; the anomalous fill also have round to asymmetrical shapes. The answer to the fill mystery may be found in the study of terrestrial pingos, as suggested by Cabrol (1999) and Sakimoto (2005). Hydraulic pingos (Figure 14) are ice mounds found in periglacial landscapes and are formed from the puncture of a groundwater source under high pressure (Soare et al., 2005). We hypothesize that the large mounds in the center of Type II craters and off-center in Type III craters may be Martian pingos. The presence of pingos implies the existence of an aquifer or another source of subterranean water. Previous studies have examined the possibility of an aquifer on Mars and have obtained a speculative depth of approximately 2 km below the surface (Hanna and Phillips, 2005a). Other studies by Hanna and Phillips suggest flooding in other areas of Mars that are due to tectonic pressurization of aquifers (Hanna and Phillips 2005b).

Figure 14: Pingo in upper Eskerdalen, Norway *The University Centre in Svalbard.* Scale is several hundred meters across the pingo. *http://www.unis.no/research/geology/Course_info/AG304info.htm*

In the pingo scenario, the aquifer must be latitude dependent based on the latitude dependences of the Type II and Type III craters. We created an aquifer model based on the predicted crater excavation depth versus latitude and then constrained it by the anomalous craters with the shallowest depths (Figure 15) to give a minimum aquifer-depth model with an equation of:

$$depth\ of\ aquifer = -0.372\,(latitude) + 3.912 \qquad \textbf{\textit{Equation 5}}$$

This model explains why Type II and Type III craters are the largest in their latitude ranges; only the largest bolides have enough energy to punch far enough into the surface and puncture the aquifer. Also, a crater of one size which punctures the aquifer at a high latitude would not necessarily be able to puncture the aquifer at a lower latitude. With this model, though, we have some craters of similar or greater depths than the Type II and Type III craters at the same latitudes which do not have these features, so the model is not without some complexity and may simply indicate that the aquifer is heterogeneous.

Figure 15: Aquifer model for the north polar region of Mars based on impact craters with anomalous fill.

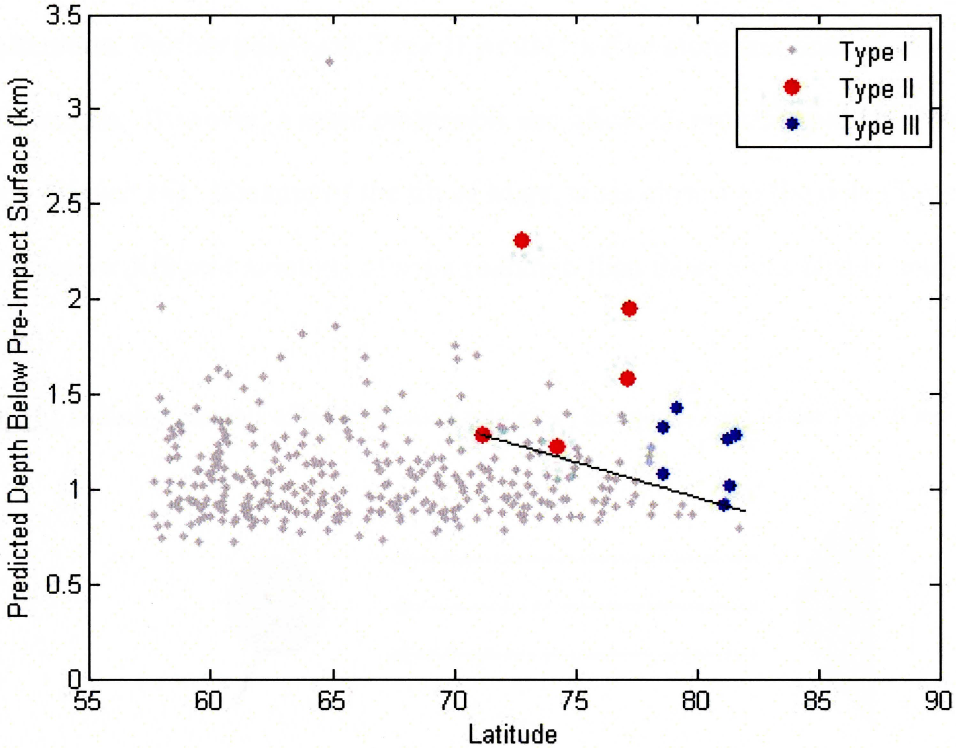

An alternate working hypothesis for the anomalous mound formation may be melting of the permafrost layer on impact rather than the puncture of an aquifer. This would explain the lack of these structures at lower latitudes whose water-rich layers are covered by soil (Litvak, 2006). Also, with this hypothesis only the largest craters have the mounds because they are the only ones which have the energy to melt a significant amount of the permafrost on impact; some large craters at high latitudes may not have these mounds because of a local variability in the amount of permafrost.

To this point, I have treated Type II and III craters in terms of one process, but they have distinctly different morphologies. To explain this difference, there are two likely: (1) they are formed by the same mechanism, but are affected by different modification processes or (2) they are formed by two different mechanisms all together.

Assuming that both Type II and III features are pingos formed by water from an aquifer or melted permafrost, subsequent modification by snow filling or melting may cause some alteration. Further poleward, Type II would receive more amounts of snow than Type III craters. However, a more reasonable modification process could be solar radiation (Figure 16). Because of the tilt of Mars, areas closest to the pole (Type III craters) receive different amounts of solar radiation than those areas farther south (Type II craters).

Figure 16: Differing amounts of solar radiation may affect the morphology of the Type II and Type III craters.

In searching for clues towards the origins and modifications of Type III craters we also examined the asymmetrical, western nature of the fill. The asymmetrical shapes suggest certain possibilities such as wind transport. On Earth, wind will deposit sediments on the lee side of a barrier. On Mars, the polar wind currents are Easterlies (Tyler and Barnes, 2005), which implies that wind would deposit sediments in the lee of the eastern rim of the crater and not on the western side like in the Type III craters. Largest in their latitude range (Figure 17), Type III craters may be able to capture more snow and dust from wind currents than their smaller counterparts.

Figure 17: Diameter vs. latitude for Type III craters and Type I craters within the latitude range of the Type III craters, clearly establishing Type III crater as the largest craters within this latitude range.

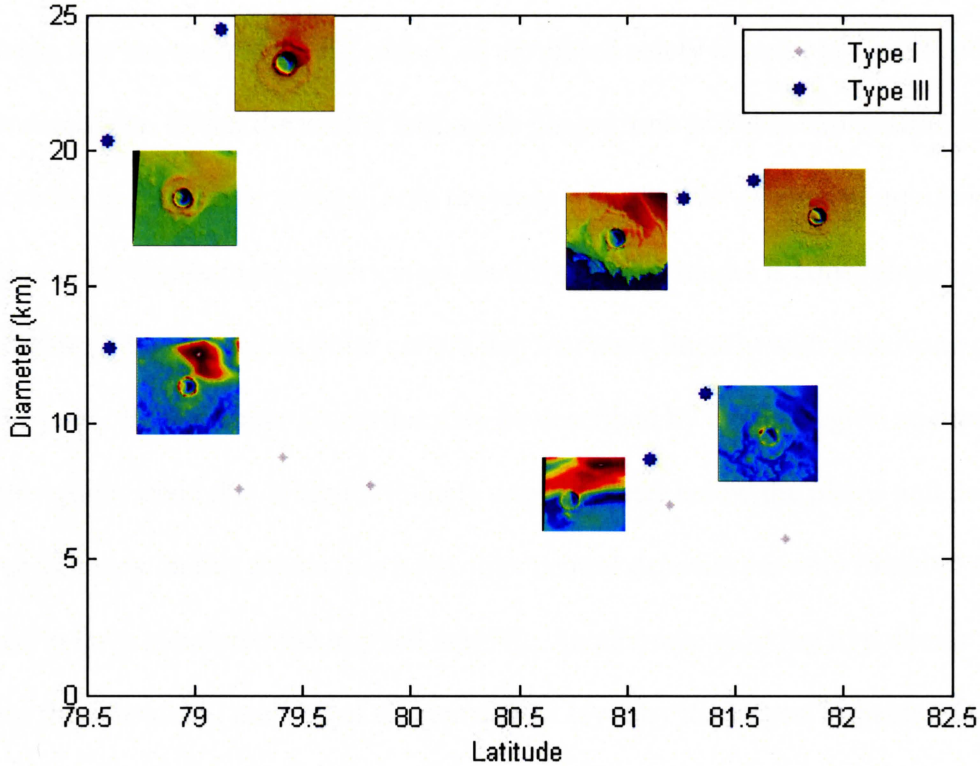

Moreover, their large diameters raise the potential for the wind to blow snow and sediments across the floor of the crater. When these sediments reach the western rim of the crater, they are unable to get over the barrier and are deposited. Fill in these craters, like Type II, are frost bright structures indicating that at least the upper-most section of the central feature is frozen water, indicating snow deposition by wind.

CONCLUSION

North polar impact craters on Mars have substantially different depth-diameter relationships than the global trends for fresh craters. When considering the polar craters with anomalous central deposits, they differ from the global population even more substantially. Specifically, their fraction of fill volume is significantly higher and they tend to form a large-diameter, high-latitude segment of the crater population. The lack of similar large central deposits in smaller craters in the same regions supports the hypothesis that the anomalous fill cannot be attributed solely to polar layered deposits, dust, and/or snow. Given the analog with earth pingos, one possible explanation for extensive fill in large polar craters is the presence of an aquifer or zone of aquifers that is pierced only by increasingly larger caters southward. This model is constrained by the crater depth of the anomalous polar craters that increases linearly with increasing distance from the pole. Impact crater properties may be described by a polar region aquifer or multiple aquifer trend that is approximately one kilometer below the plains and deepens at lower latitudes. In this model, the pingo-like central deposits are only found in craters assumed to have punctured the implied aquifer. An alternate working hypothesis involves the substantial melting of the permafrost layer by the largest impacts and subsequent pingo development. However, a difference in morphology between the Type II and Type III craters suggests another process in the north polar region. Some possible explanations towards the modification of Types II or III are differential solar radiation or wind transport. However, it is possible that Type II and Type III craters are formed from two entirely different processes and not by pingo formation. We are left, then to decide whether Type II and Type III craters are formed by the same mechanism (aquifer puncture or permafrost melting) and are subsequently modified differentially or if they are formed by two independent mechanisms. Further research is necessary to make an educated decision.

ACKNOWLEDGEMENTS

I would like to first thank Dr. Susan Sakimoto at the University of Notre Dame for giving me the jump start on this research and fueling my interest in planetary geology as a career field. I look forward to conducting research under her guidance for the next 5 years or so. I also want to thank all the professors in the Department of Geology at Washington and Lee for teaching me to ask questions, pushing me to my limits, and never letting me give up. In particular, Dr. Chris Connors has been an amazing and highly influential teacher and advisor throughout these past four years. Dr. Dave Harbor has been an equally wonderful teacher and thesis advisor. Thank you, Chris and Dave, for helping and inspiring me throughout my college career with your advice and often your silly, laid-back demeanors.

References

Ackerman, E.S. 2005. Volumetric Analysis of Martian Rampart Craters. *36th Annual Lunar and Planetary Science Conference*, March 14-18, 2005, in League City, TX, abstract no.2151.

Barlow, N.G. 2005. Martian Impact Craters as Revealed by MGS and Odyssey. *36th Annual Lunar and Planetary Science Conferenc*e, March 14-18, 2005, in League City, TX, abstract no.1415.

Boyce, J.A., P.J. Mouginis-Mark, H. Garbeil, and L.A. Soderblom. 2005. History of Major Degradational Events in the Highlands of Mars: Preliminary Results from Crater Depth/Diameter Measurements. *36th Annual Lunar and Planetary Science Conference*, March 14-18, 2005, in League City, TX, abstract no.1055.

Cabrol, N.A., E.A. Grin, and W.H. Pollard. 1997. Perennial frost mounds in Gusev crater (Mars). *28th Annual Lunar and Planetary Science Conference*, in League City, TX, abstract no.1027.

Cabrol, N.A. 1999. The Martian Impact Crater Lakes Database: A Web Resource for the Planetary Science Community and for Educational and Public Outreach. *30th Annual Lunar and Planetary Science Conference*, March 15-29, 1999, in League City, TX, abstract no. 1024.

Fenton, L.K. and K.E. Herkenhoff. 2000. Topography and Stratigraphy of the Northern Martian Polar Layered Deposits Using Photoclinometry, Stereogrammetry, and MOLA Altimetry. *Icarus*, Volume 147, Issue 2, pp. 433-443 (2000).

[A]Garvin, J.B., J.J. Frawley, S.E.H. Sakimoto, and C. Schnetzler. 2000. Global Geometric Properties of Martian Impact Craters: An Assessment from Mars Orbiter Laser Altimeter (MOLA) Digital Elevation Models. *31st Annual Lunar and Planetary Science Conference*, March 13-17, 2000, Houston, TX, abstract no. 1619.

[B]Garvin, J.B., S.E.H. Sakimoto, J.J. Frawley, and C. Schnetzler. 2000. North Polar Region Craterforms on Mars: Geometric Characteristics from the Mars Orbiter Laser Altimeter. *Icarus*, Volume 144, Issue Icarus, pp. 329-352.

Garvin, J.B., S.E.H. Sakimoto, and J.J. Frawley. 2003. Craters on Mars: Global Geometric Properties from Gridded MOLA Topography. *Sixth International Conference on Mars*, July 20-25 2003, Pasadena, California, abstract no.3277.

[A]Hanna, J.C. and R.J. Phillips. 2005. Hydrological modeling of the Martian crust with application to the pressurization of aquifers. *Journal of Geophysical Research*, Volume 110, Issue E1, CiteID E01004.

[B]Hanna, J.C. and R.J. Phillips. 2005. Tectonic Pressurization of Aquifers in the Formation of Mangala and Athabasca Valles on Mars. *36th Annual Lunar and Planetary Science Conference*, March 14-18, 2005, in League City, Texas, abstract no.2261.

Litvak, M.L., I.G. Mitrofanov, A.S. Kozyrev, A.B. Sanin, V.I. Tretyakov, W.V. Boynton, N.J. Kelly, D. Hamara, C. Shinohara, and R.S. Saunders. 2006. *Icarus*, Volume 180, Issue 1, p. 23-37.

Melosh, H.J. Impact Cratering: A Geologic Process. New York: Oxford University Press, 1989, p3, 14-16, 18.

Roark, J.H., C.M. Masuoka, and H.V. Frey. 2004. GRIDVIEW: Recent Improvements in Research and Education Software for Exploring Mars Topography. *35th Lunar and Planetary Science Conference*, March 15-19, 2004, League City, TX, abstract no.1833.

[A]Sakimoto, S.E.H. 2005. Central Mounds in Martian Impact Craters: Assessment as Possible Perennial Permafrost Mounds (Pingos). *36th Annual Lunar and Planetary Science Conference*, March 14-18, 2005, in League City, TX, abstract no.2099.

[B]Sakimoto, S.E. H. 2005. Martian Polar Craters: Possible Polar Materials Apparent Effects and Post-Impact Modification by Apparent Perrennial Permafrost Mound (Pingo) Formation. *Workshop on the Role of Volatiles and Atmospheres on Martian Impact Craters*, held July 11-14, 2005 in Laurel, Maryland. LPI Contribution No. 1273, p.94-95.

Slavney, S., R.E. Arvidson, K Eichentopf, M. Natenzon, T. Kirsanova, and V. Tarnolpolsky. 1996. The International Mars Data Base. *Lunar and Planetary Science*, volume 27, page 1215.

Soare, R.J., D.M. Burr, and J.M. Wan Bun Tseung. 2005. Possible pingos and a periglacial landscape in northwest Utopia Planitia. *Icarus*, Volume 174, Issue 2, p. 373-382.

Tyler, D. and J.R. Barnes. 2005. A mesoscale model study of summertime atmospheric circulations in the north polar region of Mars. *Journal of Geophysical Research*, Volume 110, Issue E6, CiteID E06007.

Werner, S.C., B.A. Ivanov., and G. Neukum 2005. The Martian Crater Size-Frequency Distribution and the Evolutionary History of Mars. *American Astronomical Society, DPS meeting* #37, #32.25.

Appendix A: Data

Type	Crater ID	Latitude	W Longitude	E Longitude	Elevation	Diameter	Depth I	Depth II	Rim Height	Volume	Predicted Depth I	Predicted Depth II	Filled Fraction of Crater Depth	Predicted Volume	Fill Volume
	1_2c	78.165	350.86	9.14	-4680.41	6.8105	0.15075	0.03675	0.074375	3.852	0.993332	0.92083	0.848238	18.09307	14.2411
	1_3c	78.013	319.88	40.12	-4910.34	14.2193	0.5355	0.32	0.14625	44.6531	1.321941	1.13597	0.594914	104.9604	60.3073
	2_3b	78.108	141.22	218.78	-4707.42	7.6765	0.18825	0.07875	0.081	6.6998	0.97731	0.866503	0.80738	22.61616	15.9164
	3_2b	81.732	54.765	305.235	-4882.64	5.752	0.13975	0.0165	0.111125	3.1172	0.866309	0.797506	0.838683	11.25564	8.13844
	3_3a	79.814	67.111	292.889	-5221.25	7.70225	0.3725	0.17525	0.141375	7.844	0.978915	0.867796	0.619477	22.80553	14.9615
	4_3a	81.192	198.65	161.35	-4502.83	6.985	0.1505	0.03925	0.099375	3.2065	1.013898	0.940825	0.851563	19.42615	16.2197
	5_1d	77.431	352.37	7.63	-5335.71	11.487	0.86275	0.62825	0.190625	50.419	1.190704	1.035249	0.275429	61.69882	11.2798
	5_1e	76.843	333.42	26.58	-4990.02	14.4003	0.5895	0.35275	0.17425	48.8274	1.33016	1.142202	0.55682	108.3188	59.4914
	5_2b	73.599	357.63	2.37	-5534.83	17.9825	1.021	0.7335	0.17775	139.9263	1.483129	1.256611	0.311591	188.3385	48.4122
	5_2c	74.742	346.59	13.41	-4971.6	11.978	0.543	0.2845	0.18675	43.4647	1.215376	1.054359	0.553225	68.47615	25.0114
	5_2d	74.9	345.03	14.97	-4933.19	12.3643	0.5015	0.26425	0.2045	38.3984	1.234425	1.069057	0.593738	74.10716	35.7088
	5_2e	73.023	338.06	21.94	-4768.91	12.5355	0.3815	0.17275	0.171375	29.9531	1.242773	1.075484	0.693025	76.68936	46.7363
	5_2f	72.999	332.74	27.26	-4876.28	17.669	0.6685	0.33025	0.223875	83.779	1.470403	1.247206	0.545363	180.2686	96.4896
	5_3a	70.077	346.16	13.84	-4792.11	12.5098	0.37525	0.13725	0.1895	32.5443	1.241522	1.074521	0.69775	76.29771	43.7534
	5_3c	69.49	336.86	23.14	-4556.86	7.90625	0.20125	0.02575	0.1415	6.7393	0.991535	0.877949	0.797032	24.33935	17.6001
	5_3e	68.947	333.24	26.76	-4668.44	13.9943	0.44675	0.17825	0.19225	42.4471	1.31165	1.128153	0.659398	100.8735	58.4264
	5_3i	68.524	347.07	12.93	-5095.78	14.8045	0.81675	0.45675	0.2245	74.5069	1.348328	1.155947	0.39425	116.0494	41.5425
	5_4l	65.303	1.2328	358.7672	-5019.75	8.46475	0.38325	0.1865	0.13625	13.8999	1.025259	0.90497	0.626192	28.84839	14.9485
	5_4m	65.575	356.97	3.03	-5489.75	6.44525	0.9325	0.733	0.133875	13.6864	0.949956	0.878683	0.018376	15.49683	1.81043
Type I	5_4p	63.72	349	11	-5998.29	43.5775	2.33275	1.42125	0.639125	2219.698	2.288448	1.812006	-0.01936	1706.576	513.122
	5_4r	65.083	336.63	23.37	-4436.5	6.21225	0.20075	0.0245	0.137875	4.2979	0.922042	0.851578	0.782277	13.97361	9.67571
	5_5a	61.984	353.37	6.63	-5425.97	25.4598	1.493	0.7965	0.355625	490.023	1.758616	1.455264	0.151037	447.6506	42.3724
	5_5c	62.22	334.66	25.34	-4438.28	11.5803	0.3445	0.14325	0.162125	24.5372	1.19543	1.038916	0.711819	62.95352	38.4163
	5_5e	61.461	351.09	8.91	-4777.49	9.49025	0.41425	0.1225	0.24675	18.7809	1.084348	0.951931	0.617973	38.35162	19.5707
	5_5f	61.363	341.67	18.33	-4464.02	8.157	0.22925	0.07	0.119125	5.6268	1.006821	0.890217	0.772303	26.30712	20.6803
	5_5g	61.531	338.12	21.88	-4396.17	13.203	0.417	0.07175	0.248375	47.4019	1.274771	1.10003	0.672882	87.26442	39.8625
	5_5i	61.024	335.86	24.14	-4735.05	12.2538	0.8045	0.47	0.18825	61.6069	1.229007	1.064881	0.345406	72.46899	10.8621
	5_5l	60.523	349.5	10.5	-3599.67	8.06475	0.2845	0.13175	0.127625	9.5864	1.001226	0.88573	0.715848	25.57253	15.9861
	5_5n	57.887	340.23	19.77	-5048.04	26.4335	1.26425	0.82025	0.41775	421.7655	1.791259	1.47819	0.294211	491.5045	69.739
	6_2b	77.324	219.97	140.03	-4595.8	8.933	0.27875	0.05075	0.1755	12.1831	1.052667	0.926813	0.735197	32.98722	20.8041
	6_2d	76.682	222.73	137.27	-4680.99	8.4685	0.38325	0.17575	0.157375	14.9378	1.025481	0.905147	0.626273	28.88022	13.9424
	6_2e	76.244	221.22	138.78	-4753.77	9.439	0.42575	0.2375	0.150125	20.9781	1.081474	0.949658	0.606324	37.83799	16.8599
	6_3c	71.266	228.42	131.58	-4535.98	13.307	0.342	0.1925	0.1245	31.9031	1.279681	1.103785	0.732746	88.98606	57.083
	6_3d	72.855	221.76	138.24	-4473.73	6.6435	0.1845	0.0245	0.138875	4.5356	0.973556	0.90161	0.810489	16.87387	12.3383
	6_3f	71.524	220.66	139.34	-4624.58	11.9783	0.3395	0.17675	0.12975	26.9184	1.215389	1.054369	0.720666	68.47971	41.5613
	6_3h	72.457	215.79	144.21	-5200.59	20.4383	0.98625	0.70075	0.26	189.539	1.579137	1.326904	0.37545	259.0402	69.5012
	6_3i	72.075	214.07	145.93	-5192.14	20.1015	1.1855	0.691	0.3535	192.7446	1.566334	1.317596	0.243137	248.5428	55.7982
	6_3j	72.032	210.22	149.78	-4664	9.67275	0.2885	0.115	0.1245	11.7752	1.094516	0.959963	0.736413	40.21442	28.4392
	6_4a	69.119	236.65	123.35	-4320.57	15.083	0.309	0.06925	0.1945	31.9539	1.360697	1.165281	0.772911	121.5617	89.6078

Type	Crater ID	Latitude	W Longitude	E Longitude	Elevation	Diameter	Depth I	Depth II	Rim Height	Volume	Predicted Depth I	Predicted Depth II	Filled Fraction of Crater Depth	Predicted Volume	Fill Volume
Type I	6_4b	69.93	234.12	125.88	-4303.14	8.13125	0.16975	0.04375	0.101	5.035	1.005263	0.888967	0.831139	26.10082	21.0658
	6_4c	67.674	241.57	118.43	-4308.47	9	0.23925	0.08428	0.076875	6.7831	1.056529	0.929882	0.773551	33.60673	26.8236
	6_4e	67.661	235.64	124.36	-4515.63	8.31125	0.4145	0.25725	0.114375	11.6905	1.016106	0.897652	0.59207	27.56332	15.8728
	6_4f	66.844	228.71	131.29	-4445.22	14.3525	0.39025	0.1105	0.214	38.0796	1.327997	1.140562	0.706136	107.4266	69.347
	6_4h	66.387	215.96	144.04	-5541.87	29.915	1.868	1.19475	0.605625	770.1158	1.903216	1.555859	0.018503	668.8458	101.27
	6_5d	65.43	231.66	128.34	-4713.68	21.8745	0.953	0.40725	0.48875	356.4003	1.632571	1.36553	0.416258	306.7668	49.6335
	6_5e	63.543	228.19	131.81	-4622.48	22.3278	0.77625	0.28825	0.31075	180.3519	1.64906	1.377379	0.529277	322.8393	142.487
	6_5f	65.152	216.76	143.24	-4383.55	7.08725	0.18975	0.03475	0.14275	5.0006	0.939803	0.836185	0.798096	18.53754	13.5369
	6_5g	62.132	212.48	147.52	-4348.07	9.11075	0.215	0.0835	0.09975	8.2027	1.062879	0.934925	0.797719	34.64593	26.4432
	6_6b	60.286	236.47	123.53	-4715.1	14.682	0.4985	0.28625	0.157375	59.7876	1.342849	1.151807	0.628774	113.6731	53.8855
	6_6c	60.354	230.61	129.39	-4643.04	21.5315	0.67075	0.23475	0.353875	137.4945	1.619977	1.356458	0.585951	294.9289	157.434
	6_6e	59.84	223.99	136.01	-5484.59	31.2623	1.66625	1.121	0.4335	760.3101	1.944744	1.584292	0.143203	746.3848	13.9253
	6_6f	59.396	221.82	138.18	-4554.32	13.131	0.389	0.222	0.149375	32.0076	1.27136	1.097419	0.694028	86.08429	54.0767
	6_6g	57.639	222.13	137.87	-4423.5	6.30325	0.198	0.0815	0.09025	4.0753	0.932968	0.862185	0.787774	14.55645	10.4812
	6_6i	58.698	217.97	142.03	-4455.57	6.562	0.30975	0.17475	0.088375	6.9405	0.96387	0.8922	0.678639	16.29863	9.35813
	6_6j	58.383	213.78	146.22	-4334.18	8.65025	0.24825	0.12575	0.077625	12.0724	1.036207	0.913708	0.760424	30.44835	18.3759
	6_6k	60.438	212.27	147.73	-4607.93	19.8963	0.82325	0.40125	0.335875	164.5181	1.558477	1.311874	0.47176	242.2717	77.7536
	7_1a	81.2	195.56	164.44	-4494.53	6.9695	0.15075	0.03725	0.091625	3.2572	1.012075	0.939053	0.851049	19.30526	16.0481
	7_2b	75.49	201.35	158.65	-4985.98	14.7218	0.5205	0.389	0.1145	50.7119	1.344629	1.153153	0.612905	114.4409	63.729
	7_2g	72.594	189.26	170.74	-4790.87	9.79375	0.33875	0.1345	0.158375	13.4882	1.101203	0.965238	0.692382	41.47873	27.9905
	7_2h	73.414	181.76	178.24	-5727.2	21.36	1.40125	0.99925	0.27275	271.2655	1.613642	1.351887	0.131623	289.1142	17.8487
	7_3a	71.125	202.53	157.47	-5338.26	13.7035	1.112	0.8025	0.2005	84.5062	1.298225	1.117936	0.143446	95.73546	11.2293
	7_3c	68.48	210.97	149.03	-4642.73	14.688	0.4425	0.22875	0.17425	41.3325	1.343118	1.15201	0.670543	113.7888	72.4563
	7_3e	70.237	197.68	162.32	-4806.5	11.6353	0.496	0.23375	0.2055	33.7393	1.198209	1.041071	0.586049	63.70066	29.9614
	7_3f	69.45	197.37	162.63	-4820.56	14.8505	0.51	0.295	0.161375	46.6881	1.350379	1.157496	0.622328	116.9493	70.2612
	7_3g	71.434	189.71	170.29	-5152.99	13.1663	0.5105	0.2755	0.167875	35.5943	1.273031	1.098698	0.598989	86.66086	51.0666
	7_3h	68.033	186.81	173.19	-4578.07	9.695	0.248	0.136	0.08025	8.7049	1.095749	0.960936	0.773671	40.44515	31.7402
	7_3i	69.177	183.08	176.92	-4601.59	8.754	0.1965	0.04325	0.12475	10.5923	1.042278	0.918546	0.811471	31.36582	20.7735
	7_4a	67.694	207.11	152.89	-4777.18	9.67975	0.5895	0.3695	0.179375	22.8678	1.094904	0.960269	0.461596	40.28692	17.4191
	7_4b	64.929	204.48	155.52	-4601.29	13.9563	0.6135	0.30325	0.244625	55.9151	1.309903	1.126825	0.531645	100.1928	44.2777
	7_4c	66.347	196.52	163.48	-4985.85	23.075	1.08225	0.6215	0.41425	260.4496	1.675876	1.396577	0.354218	350.4171	89.9675
	7_4e	65.129	182	178	-5683.37	46.6148	2.09825	1.3105	0.6275	2578.347	2.36526	1.861076	0.112888	2018.299	560.048
	7_5a	59.478	208.65	151.35	-4136.61	7.02875	0.65975	0.0655	0.102125	3.3978	0.935993	0.833095	0.295134	18.15887	14.7611
	7_5b	60.028	206.96	153.04	-4119.29	11.7148	0.307	0.07225	0.1925	18.217	1.202214	1.044174	0.744638	64.78995	46.5729
	7_5c	59.716	202.19	157.81	-4105.49	6.26025	0.13925	0.04375	0.075625	2.3355	0.927809	0.857177	0.849915	14.27913	11.9436
	7_5d	59.123	202.2	157.8	-4100.66	9.1645	0.267	0.0595	0.188125	9.4376	1.065947	0.937359	0.749519	35.15712	25.7195
	7_5e	58.485	201.01	158.99	-4087.6	6.746	0.1575	0.04425	0.096125	3.8124	0.985705	0.913417	0.840216	17.61568	13.8033
	7_5f	63.186	194.86	165.14	-4335.86	15.264	0.57075	0.1255	0.363125	63.3798	1.368674	1.17129	0.582991	125.2266	61.8468
	7_5g	63.545	189.77	170.23	-4607.25	15.7075	0.72825	0.3225	0.2615	60.0682	1.388018	1.185827	0.475331	134.4835	74.4153

Type	Crater ID	Latitude	W Longitude	E Longitude	Elevation	Diameter	Depth I	Depth II	Rim Height	Volume	Predicted Depth I	Predicted Depth II	Filled Fraction of Crater Depth	Predicted Volume	Fill Volume
Type I	7_5h	63.809	188.96	171.04	-4596.03	10.8515	0.4965	0.30875	0.192	24.335	1.157957	1.009759	0.571228	53.5466	29.2116
	7_5i	61.751	188.99	171.01	-4480.04	17.3488	0.685	0.2685	0.357	110.9153	1.457283	1.237489	0.529947	172.2424	61.3271
	7_5j	60.201	186.44	173.56	-4305.67	8.77175	0.24975	0.11175	0.11275	7.7192	1.043313	0.91937	0.760618	31.52442	23.8052
	7_5l	58.604	193.11	166.89	-4569.44	15.3098	0.78375	0.456	0.257125	80.9686	1.370683	1.172802	0.428205	126.1633	45.1947
	7_5m	58.72	185.31	174.69	-4652.13	19.593	0.87975	0.4495	0.34375	183.9174	1.546792	1.303351	0.431242	233.1813	49.2639
	8_1c	76.976	164.4	195.6	-5484.56	21.6203	1.1655	0.65225	0.419125	256.8851	1.623246	1.358814	0.281994	297.9652	41.0801
	8_1g	73.912	173.67	186.33	-5800.91	29.4435	1.575	1.00875	0.349625	527.3549	1.888458	1.545705	0.165986	642.9039	115.549
	8_1h	72.835	171.56	188.44	-4836.07	6.021	0.27175	0.09975	0.147	4.7092	0.898982	0.829198	0.697714	12.79817	8.08897
	8_2a	70.898	166.41	193.59	-6022.65	37.6373	2.28775	1.40975	0.67425	1430.867	2.129881	1.708622	-0.07412	1184.816	246.051
	8_2c	69.44	165.94	194.06	-4609.05	7.907	0.21225	0.0745	0.1025	6.0981	0.991581	0.877986	0.785948	24.3451	18.247
	8_2d	69.028	160.73	199.27	-4725.46	8.0065	0.415	0.194	0.164875	11.7452	0.997676	0.882881	0.584033	25.11509	13.3699
	8_2e	68.427	170.68	189.32	-5233.9	12.1068	1.0055	0.76275	0.150375	58.8027	1.22176	1.05929	0.177007	70.32359	11.5209
	8_2f	68.133	160.65	199.35	-5035.57	17.779	0.99275	0.59575	0.3145	142.5139	1.474881	1.250518	0.326895	183.0761	40.5622
	8_2g	68.167	158.37	201.63	-4678.54	13.16	0.54425	0.26075	0.20425	38.9128	1.272735	1.098472	0.572377	86.55847	47.6457
	8_2h	67.131	157.88	202.12	-4786.78	17.1223	0.7765	0.4335	0.301375	98.8169	1.447929	1.230548	0.463717	166.6974	67.8805
	8_2i	66.951	159.23	200.77	-4326.03	7.81175	0.143	0.00875	0.110875	5.032	0.98571	0.873265	0.854927	23.62141	18.5894
	8_2j	66.612	160.88	199.12	-4470.29	6.5195	0.267	0.13275	0.099375	4.4779	0.958811	0.887284	0.72153	16.00373	11.5258
	8_2k	67.285	167.09	192.91	-4880.29	14.4938	0.70225	0.4545	0.209	61.3845	1.334385	1.145402	0.473728	110.0785	48.694
	8_2l	64.827	150.58	209.42	-4982.9	22.732	1.377	0.9075	0.3615	296.7782	1.663623	1.387816	0.172288	337.5904	40.8122
	8_3a	62.901	173.19	186.81	-5725.77	36.7278	2.17475	1.46	0.506625	1395.168	2.104504	1.691813	-0.03338	1114.803	280.365
	8_3b	63.122	176.65	183.35	-4427.68	6.7135	0.328	0.1695	0.118625	6.4043	0.981856	0.909677	0.665939	17.37824	10.9739
	8_3c	62.221	180.72	179.28	-4327.5	7.049	0.17725	0.053	0.10775	3.5207	0.937314	0.834167	0.810896	18.28942	14.7687
	8_3d	61.603	168.35	191.65	-4345.02	7.411	0.215	0.12675	0.06625	5.8749	0.960599	0.85302	0.776181	20.71837	14.8435
	8_3e	61.634	165.08	194.92	-4345.68	7.3315	0.3525	0.1875	0.119625	8.4552	0.955536	0.848927	0.631097	20.16938	11.7142
	8_3f	60.653	170.34	189.66	-4624.15	17.684	0.815	0.4155	0.31775	109.3506	1.471014	1.247658	0.445961	180.65	71.2994
	8_3g	59.313	166.67	193.33	-4178.87	11.0165	0.43625	0.0985	0.25875	19.9909	1.166551	1.016463	0.626034	55.59696	35.6061
	8_3h	59.199	178.45	181.55	-4324.7	9.17725	0.23875	0.07225	0.122625	8.1732	1.066674	0.937935	0.776173	35.27903	27.1058
	8_3i	58.168	173.14	186.86	-4226.41	10.3248	0.324	0.09975	0.200125	15.1166	1.130065	0.987934	0.713291	47.30668	32.1901
	8_3j	57.618	172.81	187.19	-4213.32	11.519	0.34525	0.0875	0.19275	21.8004	1.192328	1.03651	0.71044	62.12769	40.3273
	8_3k	61.493	161.78	198.22	-4127.17	6.2095	0.14975	0.02475	0.107875	2.7152	0.921712	0.851258	0.837531	13.95624	11.241
	8_3l	60.362	162.22	197.78	-4609.72	8.201	0.742	0.54925	0.156875	16.5049	1.009479	0.892346	0.264967	26.66188	10.157
	8_3m	60.529	160.76	199.24	-4103.76	13.4875	0.383	0.0515	0.267875	28.1408	1.288157	1.110259	0.702676	92.02201	63.8812
	8_3n	60.586	157.2	202.8	-4798.13	10.796	1.06875	0.7895	0.168375	47.3604	1.155051	1.007491	0.074716	52.86728	5.50688
	9_1b	78.112	119.82	240.18	-5311.4	16.5035	0.7785	0.49725	0.187625	83.6445	1.42205	1.211287	0.452551	152.0991	68.4546
	9_2b	75.74	140.24	219.76	-4794.44	6.96625	0.21275	0.029	0.1555	5.318	1.011692	0.938681	0.789709	19.27998	13.962
	9_2c	74.095	147.62	212.38	-5277.27	10.6083	0.85325	0.475	0.324125	39.9193	1.145165	0.999763	0.254911	50.60755	10.6883
	9_2d	74.211	142.07	217.93	-5291.16	11.793	0.86875	0.551	0.221625	47.0657	1.206142	1.047216	0.279728	65.87292	18.8072
	9_2f	72.453	145.93	214.07	-4869.68	8.81225	0.43475	0.23575	0.138875	12.6302	1.045671	0.921247	0.584238	31.88809	19.2579
	9_2i	73.261	136.52	223.48	-4764.03	9.9955	0.38325	0.19075	0.136125	14.5488	1.112261	0.973947	0.655432	43.63909	29.0903

Type	Crater ID	Latitude	W Longitude	E Longitude	Elevation	Diameter	Depth I	Depth II	Rim Height	Volume	Predicted Depth I	Predicted Depth II	Filled Fraction of Crater Depth	Predicted Volume	Fill Volume
Type I	9_2j	72.849	134.92	225.08	-4607.13	7.68575	0.26175	0.07225	0.172125	7.7721	0.977887	0.866968	0.732331	22.68408	14.912
	9_2k	73.547	134.22	225.78	-4625.14	7.50725	0.25925	0.05175	0.166625	6.5689	0.966692	0.857941	0.731817	21.39488	14.826
	9_2l	73.954	128.72	231.28	-4636	8.66425	0.2815	0.06675	0.187125	8.1122	1.037028	0.914363	0.728551	30.5712	22.459
	9_2m	72.672	120.92	239.08	-4561.52	7.58	0.17025	0.04575	0.117	4.775	0.971271	0.861635	0.824714	21.91486	17.1399
	9_2n	75.909	128.78	231.22	-4936.77	7.1015	0.419	0.128	0.246625	8.6643	0.940728	0.836936	0.5546	18.63048	9.96618
	9_3a	71.64	124.19	235.81	-4836.89	14.8655	0.80975	0.4595	0.254625	72.0902	1.351047	1.158001	0.40065	117.2437	45.1535
	9_3b	70.211	123.78	236.22	-4085.47	8.4675	0.35575	0.0885	0.19675	8.9004	1.025422	0.9051	0.65307	28.87173	19.9713
	9_3d	68.324	124.57	235.43	-4687.84	10.3908	0.969	0.63425	0.243375	42.3622	1.133599	0.990705	0.1452	48.06325	5.70105
	9_3g	69.579	140.42	219.58	-4789.22	13.5828	0.6795	0.41125	0.16575	49.7601	1.292607	1.113654	0.474318	93.64871	43.8886
	9_3h	68.708	147.67	212.33	-4541.54	12.8173	0.4745	0.209	0.21925	43.6138	1.256383	1.08594	0.622328	81.05346	37.4397
	9_3k	67.767	137.29	222.71	-4815.77	14.6438	0.8985	0.649	0.21325	76.7483	1.341134	1.15051	0.330045	112.9371	36.1888
	9_3l	68.328	133.43	226.57	-4233.97	8.043	0.232	0.0525	0.1485	7.511	0.999902	0.884668	0.767977	25.40115	17.8901
	9_3n	64.221	139.1	220.9	-4332.24	14.1093	0.7795	0.56175	0.15625	54.17	1.31692	1.132158	0.408089	102.9502	48.7802
	9_3o	64.806	137.04	222.96	-3850.01	5.59725	0.12775	0.0075	0.0955	1.5671	0.847381	0.779158	0.849241	10.42529	8.85819
	9_3q	64.46	126.47	233.53	-4458.07	14.0558	1.13525	0.81675	0.20225	77.9815	1.314471	1.130297	0.136345	101.9809	23.9994
	9_4a	63.915	140.27	219.73	-4390.35	14.1643	0.8815	0.6115	0.219125	58.7558	1.319433	1.134066	0.33191	103.9524	45.1966
	9_4b	62.6	139.27	220.73	-3970.16	14.7433	0.63275	0.333	0.243	67.6918	1.345591	1.15388	0.529761	114.8575	47.1657
	9_4c	62.671	138.53	221.47	-4199.36	16.6033	0.911	0.57125	0.26475	92.1297	1.426255	1.214423	0.361264	154.3986	62.2689
	9_4d	62.866	133.65	226.35	-3973.34	13.4155	0.65	0.4115	0.22475	49.0547	1.284783	1.107683	0.494078	90.80369	41.749
	9_4e	63.924	127.73	232.27	-3916.78	6.43625	0.488	0.31325	0.132375	6.3948	0.948881	0.877639	0.48571	15.4361	9.0413
	9_4f	63.062	127.34	232.66	-3646.67	10.752	0.3765	0.16475	0.156	13.8797	1.152742	1.005687	0.673388	52.3324	38.4527
	9_4i	59.947	125.92	234.08	-3149.88	6.263	0.18175	0.02425	0.131	2.7275	0.928139	0.857497	0.804178	14.29676	11.5693
	9_4j	59.834	131.94	228.06	-3319.74	9.363	0.30975	0.09225	0.18075	12.0682	1.077199	0.946275	0.712449	37.08393	25.0157
	9_4k	59.59	132.68	227.32	-3742.05	15.2485	0.75425	0.53125	0.199	61.0126	1.367993	1.170777	0.448645	124.9102	63.8976
	9_4l	61.708	131.01	228.99	-4339.06	19.8583	1.23625	0.93625	0.252375	246.9058	1.557018	1.310811	0.206014	241.1212	5.78459
	9_4m	60.266	138.32	221.68	-4159.05	17.1158	1.00825	0.72575	0.211625	108.7227	1.44766	1.230348	0.303531	166.5399	57.8172
	9_4n	60.081	146.18	213.82	-4149.9	15.0738	0.74275	0.48425	0.1425	61.9694	1.360288	1.164973	0.453976	121.3762	59.4068
	9_4o	59.551	151.14	208.86	-3801.18	8.33625	0.23725	0.023	0.18825	7.2883	1.017602	0.898849	0.766854	27.77023	20.4819
	10_1a	78.128	119.84	240.16	-5345.98	16.764	0.79425	0.5045	0.17375	81.0847	1.433004	1.219451	0.445745	158.1476	77.0629
	10_1b	76.082	121.77	238.23	-4811.48	7.92775	0.245	0.05325	0.166375	7.7548	0.992855	0.87901	0.753237	24.50449	16.7497
	10_1c	76.421	94.797	265.203	-4841.74	10.5315	0.34925	0.06325	0.244	15.6402	1.141097	0.996579	0.693935	49.70076	34.0606
	10_1d	76.149	89.438	270.562	-5324.07	6.8395	0.5425	0.49725	0.1055	8.8094	0.996756	0.92416	0.455735	18.31039	9.50099
	10_2a	73.838	101.81	258.19	-4738.77	12.3458	0.3655	0.17325	0.1315	23.1148	1.23352	1.06836	0.703693	73.83137	50.7166
	10_2d	73.074	105.88	254.12	-4704.93	15.426	0.53475	0.283	0.190875	50.9912	1.375773	1.176631	0.611309	128.5622	77.571
	10_2e	72.415	112.44	247.56	-4717.25	11.2708	0.6085	0.37	0.156	30.0214	1.179667	1.026674	0.484176	58.84708	28.8257
	10_2g	70.518	118.82	241.18	-4356.45	9.3355	0.27925	0.12075	0.103375	14.6683	1.075647	0.945047	0.740389	36.81332	22.145
	10_2h	69.351	114.6	245.4	-4302.93	11.5373	0.427	0.205	0.179625	25.0248	1.193253	1.037228	0.642155	62.37307	37.3483
	10_2i	70.049	110.88	249.12	-4119.39	7.30875	0.20275	0.035	0.136375	4.6055	0.954082	0.847751	0.787492	20.0139	15.4084
	10_2j	71.065	111.12	248.88	-4677.86	10.9845	0.55225	0.428	0.093375	27.1443	1.16489	1.015168	0.525921	55.19571	28.0514

Type	Crater ID	Latitude	W Longitude	E Longitude	Elevation	Diameter	Depth I	Depth II	Rim Height	Volume	Predicted Depth I	Predicted Depth II	Filled Fraction of Crater Depth	Predicted Volume	Fill Volume
Type I	10_2m	70.951	105.38	254.62	-4334.27	7.27725	0.2965	0.1505	0.09475	5.501	0.952065	0.846119	0.688572	19.79981	14.2988
	10_2o	71.979	101.75	258.25	-4398.64	6.38425	0.21475	0.04775	0.124125	4.1825	0.942667	0.871604	0.772189	15.08822	10.9057
	10_2r	70.309	93.59	266.41	-5257.63	26.7858	1.4605	0.947	0.40175	443.7921	1.802915	1.486346	0.189923	507.9756	64.1835
	10_3a	67.248	110.62	249.38	-4609.4	23.7025	1.38175	0.8805	0.376625	323.4528	1.698055	1.41239	0.186275	374.6277	51.1749
	10_3b	66.963	107.95	252.05	-3874.13	9.62675	0.372	0.1875	0.149	14.4853	1.091962	0.957947	0.659329	39.7399	25.2546
	10_3d	65.144	116.19	243.81	-3748.15	9.34225	0.282	0.121	0.108625	8.4084	1.076028	0.945348	0.737925	36.87963	28.4712
	10_3h	64.195	109.55	250.45	-3978.46	14.6208	0.7775	0.5395	0.161	52.7711	1.340101	1.149729	0.41982	112.4959	59.7248
	10_3i	62.587	114.36	245.64	-4199.62	17.0535	1.215	0.88025	0.263125	130.2358	1.445077	1.22843	0.159215	165.0358	34.8
	10_3k	62.103	121.81	238.19	-3954.86	31.3693	1.40175	0.948	0.315125	676.6129	1.948003	1.586515	0.280417	752.762	76.1491
	10_3l	65.47	92.702	267.298	-3747.18	10.3065	0.2585	0.04375	0.17125	14.0059	1.129086	0.987166	0.771054	47.09874	33.0928
	10_3m	64.561	93.149	266.851	-3615.37	9.33125	0.2335	0.0265	0.152125	9.5356	1.075407	0.944857	0.782873	36.7716	27.236
	10_3n	64.442	92.495	267.505	-3889.55	7.753	0.49525	0.35725	0.10625	11.7612	0.982071	0.870337	0.495708	23.18153	11.4203
	10_3o	62.394	93.774	266.226	-3408.4	11.4408	0.383	0.149	0.198625	28.7229	1.188352	1.033424	0.677705	61.08212	32.3592
	10_3p	65.278	102.17	257.83	-3518.09	6.28625	0.1265	0.011	0.1025	3.6629	0.930929	0.860206	0.864114	14.4464	10.7835
	10_4c	60.526	120.85	239.15	-3277.38	9.893	0.33675	0.14925	0.150125	15.7048	1.106657	0.969536	0.695705	42.5333	26.8285
	10_4d	58.683	115.51	244.49	-3152.01	20.9375	0.84175	0.68425	0.14425	157.0211	1.597922	1.340523	0.473222	275.0839	118.063
	10_4e	58.636	110.85	249.15	-3313.52	21.0815	0.775	0.63725	0.070125	134.9236	1.603298	1.344413	0.516621	279.819	144.895
	10_4f	60.154	108.85	251.15	-3572.99	21.856	0.953	0.628	0.3195	214.8895	1.631895	1.365043	0.416016	306.1212	91.2317
	10_4g	58.323	103.15	256.85	-3343.79	19.884	1.21375	0.84175	0.2615	208.3409	1.558007	1.311532	0.22096	241.9005	33.5596
	10_4h	60.713	101.43	258.57	-4246.07	21.697	1.724	1.30075	0.35275	324.2902	1.626067	1.360847	-0.06023	300.606	23.6842
	10_4i	60.106	96.779	263.221	-2952.03	13.6778	0.5385	0.22725	0.204375	40.6463	1.297029	1.117025	0.58482	95.28815	54.6418
	10_4j	59.478	96.361	263.639	-2609.32	13.2505	0.41875	0.09375	0.264	36.6462	1.277016	1.101747	0.672087	88.04825	51.4021
	10_4k	58.447	94.893	265.107	-2493.81	18.846	0.714	0.209	0.335	106.1884	1.517609	1.281988	0.529523	211.6694	105.481
	10_4l	60.322	88.433	271.567	-3688.54	13.895	0.80275	0.56	0.191125	61.7155	1.307083	1.12468	0.385846	99.10149	37.386
	11_2a	75.149	88.322	271.678	-5069.12	15.3708	0.5635	0.26475	0.225375	56.8411	1.373356	1.174813	0.589691	127.4187	70.5776
	11_2b	74.784	83.593	276.407	-4875.14	7.41125	0.1865	0.018	0.139625	6.1228	0.960615	0.853033	0.805854	20.72011	14.5973
	11_2d	73.04	76.542	283.458	-4985.03	8.42375	0.1385	0.0395	0.062375	6.0717	1.022822	0.903023	0.86459	28.50172	22.43
	11_2e	72.16	81.544	278.456	-2418.36	9.3695	0.2165	0.03125	0.148125	10.086	1.077565	0.946565	0.799084	37.14807	27.0621
	11_2g	69.278	86	274	-5149.2	12.4803	1.3025	1.04125	0.1805	78.2969	1.240086	1.073416	-0.05033	75.85049	2.44641
	11_2h	68.834	86.19	273.81	-4580.22	9.07575	0.446	0.23575	0.122125	13.7117	1.060877	0.933335	0.579593	34.31546	20.6038
	11_2i	68.215	84.11	275.89	-4562.66	12.7318	0.42575	0.1675	0.187	33.6555	1.252269	1.082782	0.660017	79.71385	46.0583
	11_2j	70.365	77.253	282.747	-4944.32	10.2498	0.325	0.15275	0.11775	13.1107	1.126035	0.984772	0.711377	46.45564	33.3449
	11_2k	69.878	74.988	285.012	-5720.42	21.464	1.211	0.935	0.25225	253.1883	1.617487	1.354662	0.251308	292.6321	39.4438
	11_2o	72.418	74.259	285.741	-4930.28	8.7295	0.16975	0.022	0.117375	4.351	1.040848	0.917406	0.836912	31.1477	26.7967
	11_2r	74.469	69.945	290.055	-5012	9.44275	0.22975	0.02925	0.155375	8.6286	1.081685	0.949825	0.7876	37.87544	29.2468
	11_3a	65.492	76.313	283.687	-5350.66	22.0215	1.46875	1.085	0.32325	300.8289	1.637938	1.36939	0.103293	311.9257	11.0968
	11_3b	65.125	77.177	282.823	-4569.11	9.6485	0.259	0.36025	0.157375	9.9865	1.09317	0.958901	0.763074	39.96385	29.9773
	11_3c	65.073	78.928	281.072	-4228.63	12.3275	0.3365	0.10775	0.15425	18.9555	1.232626	1.067671	0.727006	73.55991	54.6044
	11_3d	64.655	77.06	282.94	-4429.24	10.0998	0.4555	0.2805	0.133375	21.5886	1.11793	0.978406	0.592551	44.78121	23.1926

Type	Crater ID	Latitude	W Longitude	E Longitude	Elevation	Diameter	Depth I	Depth II	Rim Height	Volume	Predicted Depth I	Predicted Depth II	Filled Fraction of Crater Depth	Predicted Volume	Fill Volume
Type I	11_3e	63.294	76.862	283.138	-4830.14	11.3795	1.037	0.80725	0.187375	47.5164	1.185231	1.030999	0.125065	60.2711	12.7547
	11_3f	63.113	81.253	278.747	-3824.86	8.64925	0.20275	0.021	0.14925	8.3563	1.036148	0.913661	0.804323	30.43959	22.0833
	11_3g	62.996	84.289	275.711	-3713.94	7.021	0.174	0.06125	0.091125	4.7404	0.935488	0.832685	0.814001	18.10906	13.3687
	11_3i	61.456	89.862	270.138	-3280.18	8.602	0.25725	0.04525	0.145	8.9335	1.033371	0.911446	0.751057	30.02721	21.0937
	11_3k	60.251	79.285	280.715	-4906.94	33.681	1.85625	1.299	0.422875	1002.337	2.017071	1.633334	0.07973	898.5681	103.769
	11_3l	60.207	76.477	283.523	-4053.98	15.4398	0.6125	0.31225	0.246375	77.3468	1.376373	1.177082	0.55499	128.8477	51.5009
	11_3p	63.824	64.202	295.798	-5206.1	19.3423	0.85575	0.5835	0.1995	133.9832	1.53706	1.296239	0.443255	225.8212	91.838
	11_3q	63.765	67.903	292.097	-5786.8	17.0948	1.5995	1.30075	0.1815	161.1696	1.446789	1.229702	-0.10555	166.0316	4.86196
	11_3r	66.565	64.068	295.932	-5048.65	9.636	0.24625	0.0685	0.12325	12.083	1.092476	0.958353	0.774595	39.83505	27.7521
	11_3s	66.52	62.36	297.64	-5160.96	9.902	0.314	0.12925	0.12875	18.0219	1.107151	0.969924	0.716389	42.62972	24.6078
	12_1a	79.205	36.234	323.766	-5228.95	7.57275	0.3775	0.18275	0.156875	8.2853	0.970816	0.861268	0.611152	21.86271	13.5774
	12_1b	76.899	54.915	305.085	-5547.52	22.7715	1.08925	0.40225	0.48175	200.2139	1.665039	1.388829	0.345811	339.053	138.839
	12_2b	69.635	60.824	299.176	-5137.47	6.50375	0.212	0.046	0.12625	4.0399	0.956934	0.885461	0.778459	15.89533	11.8554
	12_2f	67.266	55.549	304.451	-5262.83	11.2923	0.26175	0.131	0.113375	15.576	1.180769	1.027531	0.778322	59.12699	43.551
	12_2g	64.164	49.31	310.69	-5179.61	11.5805	0.346	0.177	0.109375	20.906	1.195443	1.038926	0.710568	62.95691	42.0509
	12_2h	64.546	44.096	315.904	-5890.67	12.6428	1.0945	0.86225	0.161875	62.16	1.247972	1.079481	0.122977	78.33356	16.1736
	12_2k	65.664	30.566	329.434	-5449.84	18.5355	0.48925	0.303	0.137375	93.7706	1.505305	1.27295	0.674983	203.0921	109.322
	12_2t	73.791	37.153	322.847	-5188.75	9.0295	0.224	0.017	0.18425	7.5446	1.058224	0.931229	0.788325	33.88169	26.3371
	12_3a	63.175	60.953	299.047	-4869.07	8.30025	0.36125	0.22475	0.10275	10.6811	1.015447	0.897125	0.644245	27.47258	16.7915
	12_3c	60.474	58.283	301.717	-5011.5	9.17975	0.5595	0.442	0.0655	19.6828	1.066816	0.938048	0.475542	35.30297	15.6202
	12_3d	59.888	57.523	302.477	-4837.09	12.7593	0.46175	0.2495	0.148625	35.9928	1.253594	1.083799	0.631659	80.14326	44.1505
	12_3e	59.399	57.491	302.509	-5882.58	24.4705	1.73275	1.28475	0.351125	478.6237	1.724795	1.431375	-0.00461	405.5861	73.0376
	12_3g	60.521	46.919	313.081	-5504.7	18.2508	0.98675	0.64225	0.25575	134.7175	1.493929	1.264576	0.339494	195.4121	60.6946
	12_3h	61.355	48.546	311.454	-6145.18	28.7213	1.647	1.27325	0.3025	622.8414	1.865615	1.529939	0.117181	604.3502	18.4912
	12_3i	61.587	51.997	308.003	-5870.32	20.2883	1.34125	1.0555	0.1945	233.7661	1.573448	1.32277	0.147573	254.3322	20.5661
	12_3l	63.407	46.264	313.736	-5560.66	10.1858	0.75	0.5495	0.1425	30.5665	1.122585	0.982063	0.331899	45.73672	15.1702
	12_3n	63.041	39.845	320.155	-5310.8	18.5445	0.48575	0.27675	0.15975	94.3755	1.505663	1.273213	0.677385	203.3378	108.962
	13_1a	79.404	310.81	49.19	-4644.38	8.75875	0.24925	0.09875	0.113625	9.152	1.042555	0.918767	0.760924	31.40822	22.2562
	13_1d	78.009	307.63	52.37	-4717.46	15.224	0.438	0.185	0.2335	59.1821	1.366915	1.169966	0.67957	124.4111	65.229
	13_1g	76.654	313.64	46.36	-4605.05	11.7515	0.3095	0.07275	0.17075	17.7128	1.20406	1.045604	0.742953	65.29722	47.5844
	13_2c	72.989	321.69	38.31	-5399.26	11.0353	1.23175	0.93075	0.212625	55.8291	1.167524	1.017221	-0.05501	55.83288	0.00378
	13_2e	72.185	320.63	39.37	-4503.55	9.71875	0.20275	0.02975	0.143625	9.2551	1.097063	0.961973	0.815188	40.69231	31.4372
	13_2f	70.184	318.64	41.36	-4537.23	5.82075	0.2525	0.12225	0.0975	3.7192	0.874686	0.80563	0.711325	11.63778	7.91858
	13_2h	70.663	302.44	57.56	-4581.26	12.7805	0.37775	0.232	0.11975	32.6498	1.254616	1.084585	0.698912	80.47603	47.8262
	13_2l	73.583	297.94	62.06	-4956.15	6.9285	0.78325	0.58675	0.13325	11.3619	1.00725	0.934361	0.222387	18.98783	7.62593
	13_3b	69.379	318.47	41.53	-4916.14	21.1365	0.89775	0.4965	0.32475	193.9352	1.605346	1.345894	0.440775	281.6403	87.7051
	13_3e	66.317	320.22	39.78	-5696.28	36.8015	2.1785	1.3455	0.679375	1363.103	2.106573	1.693186	-0.03414	1120.386	242.717
	13_3f	64.916	328.79	31.21	-4857.49	21.9785	0.96525	0.506	0.365125	225.3752	1.63637	1.368263	0.410127	310.4113	85.0361
	13_3g	65.3	327.54	32.46	-4326.97	7.14275	0.17825	0.05675	0.094875	3.8206	0.943402	0.839103	0.811056	18.90111	15.0805

Type	Crater ID	Latitude	W Longitude	E Longitude	Elevation	Diameter	Depth I	Depth II	Rim Height	Volume	Predicted Depth I	Predicted Depth II	Filled Fraction of Crater Depth	Predicted Volume	Fill Volume
Type I	13_3h	64.079	325.6	34.4	-4507.62	10.0768	0.39275	0.20875	0.13425	15.7438	1.116682	0.977424	0.648288	44.52771	28.7839
	13_3j	66.105	313.26	46.74	-4385.64	5.3985	0.1345	0.0555	0.0465	2.006	0.822925	0.755463	0.836559	9.418172	7.41217
	13_3k	67.191	312.18	47.82	-4550.74	14.3435	0.38675	0.17125	0.183	47.2561	1.327589	1.140253	0.708682	107.259	60.0029
	13_3n	67.077	304.91	55.09	-4605.26	5.2075	0.42525	0.2865	0.123875	3.8981	0.799262	0.732548	0.467946	8.511526	4.61343
	13_3o	66.381	305.31	54.69	-4331.69	6.136	0.148	0.03375	0.084625	2.1888	0.912865	0.84267	0.837873	13.49699	11.3082
	13_4b	60.912	328.9	31.1	-4251.18	5.99175	0.2355	0.07275	0.123625	3.6469	0.895443	0.825764	0.737002	12.62423	8.97733
	13_4c	57.97	323.6	36.4	-4013.79	5.30725	0.192	0.0585	0.083833	2.9282	0.81164	0.744533	0.763442	8.977649	6.04945
	13_4d	58.198	321.37	38.63	-4574.79	5.894	0.76	0.625	0.10025	0.87065	0.883591	0.814267	0.139874	12.05401	11.1834
	13_4f	59.473	321.92	38.08	-4283.99	5.144	0.43425	0.238	0.1475	4.6413	0.791358	0.724898	0.45126	8.223087	3.58179
	13_4g	61.602	322.66	37.34	-4271.76	9.49275	0.3185	0.09175	0.158375	15.6877	1.084488	0.952041	0.706313	38.37678	22.6891
	13_4h	62.921	317.8	42.2	-4291.99	5.70675	0.181	0.0885	0.073125	2.3591	0.860784	0.79215	0.789727	11.00859	8.64949
	13_4i	61.785	318.71	41.29	-4236.77	11.3783	0.29275	0.01925	0.204375	20.6449	1.185167	1.030949	0.752988	60.25461	39.6097
	13_4j	60.988	316.77	43.23	-4321.07	7.327	0.29	0.12975	0.131125	8.7264	0.955248	0.848695	0.696414	20.13857	11.4122
	13_4k	59.379	309.64	50.36	-4211.92	6.8875	0.33675	0.15475	0.148875	9.0826	1.002419	0.929664	0.664063	18.67378	9.59118
	13_4l	59.662	307.21	52.79	-4247.14	11.0228	0.39625	0.14125	0.235625	25.5757	1.166876	1.016716	0.660418	55.67553	30.0998
	13_4m	60.039	313.5	46.5	-4285.95	12.989	0.47875	0.24375	0.166875	39.4614	1.264604	1.092245	0.621423	83.78493	44.3235
	13_4p	61.958	301.77	58.23	-4233.86	8.57225	0.33375	0.1465	0.144375	14.7581	1.031618	0.910047	0.676479	29.76929	15.0112
	14_1b	76.336	27.262	332.738	-5244.98	12.1435	0.343	0.12925	0.180125	30.4683	1.223576	1.060692	0.719674	70.85633	40.388
	14_1c	75.053	19.787	340.213	-5357.31	16.6495	0.4725	0.26625	0.165625	62.7636	1.4282	1.215872	0.669164	155.4717	92.7081
	14_1e	75.226	14.433	345.567	-5053.7	7.528	0.1895	0.02825	0.1425	6.9693	0.968	0.858997	0.804236	21.54243	14.5731
	14_1f	74.631	13.094	346.906	-5386.02	22.989	0.78125	0.4495	0.196875	205.8469	1.672813	1.394389	0.532972	347.1742	141.327
	14_1j	74.249	359.92	0.08	-4862.8	7.25375	0.17125	0.0225	0.112875	5.4038	0.950557	0.844899	0.819842	19.64098	14.2372
	14_2a	72.508	19.385	340.615	-5213.9	13.194	0.351	0.13475	0.183375	28.9943	1.274345	1.099704	0.724564	87.11638	58.1221
	14_2b	71.907	15.181	344.819	-6070.11	20.2485	1.4255	1.03975	0.258875	246.7695	1.571937	1.321672	0.093157	253.0933	6.32377
	14_2c	71.947	25.223	334.777	-5240.56	11.692	0.33125	0.07125	0.23	21.8665	1.201069	1.043287	0.724204	64.4771	42.6106
	14_2d	71.003	27.897	332.103	-5176.73	10.2973	0.18975	0.01425	0.155625	10.5505	1.128589	0.986776	0.83187	46.99356	36.4431
	14_2e	70.277	28.363	331.637	-5391.51	16.0828	0.406	0.18875	0.16225	55.0433	1.404168	1.197928	0.710861	142.6263	87.583
	14_2j	69.321	21.727	338.273	-5167.13	5.60225	0.15675	0.03075	0.097	2.0958	0.847994	0.779752	0.815152	10.45148	8.35568
	14_2l	70.328	18.65	341.35	-5148.76	10.6923	0.26075	0.05	0.1905	15.1557	1.149599	1.00323	0.773182	51.61126	36.4556
	14_2m	73.535	11.746	348.254	-5415.92	15.9955	0.57225	0.3625	0.172875	83.8639	1.40043	1.19513	0.591376	140.7074	56.8435
	14_2n	72.067	5.2144	354.7856	-5153.39	5.61325	0.43075	0.2815	0.11625	5.7071	0.849343	0.781059	0.492843	10.50925	4.80215
	14_2p	70.049	7.9485	352.0515	-6024.9	40.252	2.2055	1.6085	0.505875	1701.797	2.201144	1.755434	-0.00198	1400.5	301.297
	14_2q	69.202	3.6248	356.3752	-5111.37	5.57875	0.39725	0.2445	0.1175	4.5961	0.845112	0.776959	0.529944	10.32875	5.73265
	14_2r	68.743	1.1213	358.8787	-5034.72	6.89475	0.31475	0.1825	0.109	7.8053	1.003273	0.930495	0.686277	18.72907	10.9238
	14_3a	67.53	26.047	333.953	-5126.42	8.68425	0.19325	0.01475	0.1575	6.7822	1.038201	0.915297	0.813861	30.74722	23.965
	14_3b	66.966	21.346	338.654	-5190.31	6.476	0.14275	0.02925	0.083125	3.6567	0.953625	0.882247	0.850308	15.70549	12.0488
	14_3c	66.912	16.281	343.719	-5404.27	13.1848	0.45525	0.317	0.106375	34.4472	1.273907	1.099369	0.642635	86.96438	52.5172
	14_3d	65.628	21.227	338.773	-5804.42	19.5093	0.8355	0.66125	0.163	143.8846	1.543549	1.300982	0.458715	230.7073	86.8227
	14_3e	63.162	20.88	339.12	-5194.31	8.4945	0.23225	0.058	0.1395	9.4782	1.027023	0.906379	0.773861	29.10151	19.6233

Type	Crater ID	Latitude	W Longitude	E Longitude	Elevation	Diameter	Depth I	Depth II	Rim Height	Volume	Predicted Depth I	Predicted Depth II	Filled Fraction of Crater Depth	Predicted Volume	Fill Volume
Type I	14_3i	62.409	23.62	336.38	-5110.61	9.0865	0.2025	0.05	0.117	7.8253	1.061492	0.933824	0.809231	34.41676	26.5915
	14_3k	63.177	20.716	339.284	-5586.42	10.9815	0.72475	0.51525	0.167375	38.9164	1.164734	1.015046	0.377755	55.15818	16.2418
	14_3l	62.586	15.409	344.591	-5067.62	8.386	0.204	0.0365	0.1335	7.9463	1.020574	0.901225	0.800112	28.18474	20.2384
	14_3m	62.983	13.475	346.525	-5214.14	6.78425	0.3635	0.2085	0.121125	7.3221	0.990229	0.917815	0.632913	17.89779	10.5757
	14_3p	65.307	1.23	358.77	-5017.45	8.39175	0.38525	0.1605	0.18275	12.548	1.020917	0.9015	0.622643	28.23288	15.6849
	14_4h	59.173	8.163	351.837	-5076.37	5.882	0.366	0.194	0.13125	6.2416	0.882134	0.812853	0.585097	11.98518	5.74358
	14_4j	61.218	1.8878	358.1122	-5034.03	11.7883	0.4575	0.2245	0.166625	26.1355	1.205904	1.047032	0.620617	65.80687	39.6714
	15_1d	74.611	287.72	72.28	-4373.71	9.35225	0.189	0.0185	0.15425	11.0287	1.076593	0.945795	0.824446	36.97801	25.9493
	15_1e	76.118	269.48	90.52	-4383.61	10.8068	0.2445	0.0885	0.105	14.8847	1.155615	1.007931	0.788424	52.99845	38.1138
	15_2c	71.985	292.03	67.97	-4475.33	19.918	0.43275	0.184	0.21	76.8567	1.559312	1.312482	0.722474	242.9317	166.075
	15_2e	69.791	295.15	64.85	-4421.03	17.9445	0.39875	0.13575	0.204125	69.1348	1.481593	1.255476	0.730864	187.349	118.214
	15_2f	69.487	294.09	65.91	-4584.29	11.078	0.54175	0.32175	0.175625	27.6185	1.169738	1.018946	0.536862	56.373	28.7545
	15_2h	69.677	290.84	69.16	-4468.97	6.173	0.39475	0.244	0.109875	6.552	0.917321	0.846995	0.569671	13.72694	7.17494
	15_2k	71.414	273.86	86.14	-4139.02	8.109	0.1475	0.02075	0.100125	6.7364	1.003914	0.887886	0.853075	25.92334	19.1869
	15_3a	67.143	296.88	63.12	-4421.4	10.9773	0.34175	0.1665	0.1505	23.7132	1.164513	1.014874	0.70653	55.10504	31.3918
	15_3f	62.361	293.03	66.97	-4009.66	6.98175	0.19925	0.0565	0.103	4.8848	1.013515	0.940454	0.803407	19.40076	14.516
	15_3g	64.469	292.7	67.3	-4042.04	18.064	0.4335	0.0275	0.36875	90.7273	1.486419	1.259039	0.70836	190.4711	99.7438
	15_3h	64.437	291.36	68.64	-4089.23	8.99425	0.234	0.08525	0.0985	11.284	1.056198	0.929619	0.778451	33.55329	22.2693
	15_3i	64.329	289.63	70.37	-4001.28	7.36625	0.17725	0.02275	0.122	6.1245	0.957752	0.85072	0.814931	20.40826	14.2838
	15_3j	65.137	289.22	70.78	-4350.87	12.7375	0.55	0.344	0.14475	38.224	1.252546	1.082995	0.560894	79.80352	41.5795
	15_3k	67.758	284.67	75.33	-4151.22	7.48625	0.2165	0.069	0.11975	7.292	0.965366	0.85687	0.775733	21.24617	13.9542
	15_3l	66.981	271.24	88.76	-4703.07	13.1405	1.07825	0.7825	0.217875	73.9055	1.27181	1.097764	0.152193	86.23945	12.334
	15_3m	66.159	278.53	81.47	-3955.62	17.7835	0.53275	0.05275	0.39325	82.8115	1.475064	1.250653	0.638829	183.1915	100.38
	15_3n	64.604	281.14	78.86	-3993.41	8.88175	0.29375	0.10025	0.1715	9.488	1.049704	0.924456	0.720159	32.518	23.03
	15_3o	63.478	279.76	80.24	-3987.23	6.4485	0.246	0.1325	0.08625	5.2698	0.950344	0.87906	0.741146	15.5188	10.249
	15_3p	62.344	278.3	81.7	-3961.96	10.146	0.295	0.10825	0.156	15.8998	1.120436	0.980375	0.73671	45.29357	29.3938
	15_4a	61.688	289.28	70.72	-4005.73	12.266	0.4325	0.184	0.184875	27.0385	1.229609	1.065345	0.648262	72.64952	45.611
	15_4b	57.911	301.34	58.66	-5003.84	53.1305	2.25725	1.46	0.700125	3549.082	2.52186	1.959106	0.104927	2795.559	753.523
	15_4c	58.078	297.83	62.17	-4701.21	23.5283	1.34	0.87625	0.3785	396.657	1.691926	1.408026	0.208003	367.8075	28.8495
	15_4d	58.271	292.3	67.7	-3938.84	14.924	0.502	0.17875	0.251	52.8672	1.35365	1.159966	0.629151	118.3959	65.5287
	15_4g	58.22	285.26	74.74	-4344.98	18.2765	0.89325	0.60975	0.211875	138.5773	1.494962	1.265336	0.402493	196.0993	57.522
	15_4h	60.445	283.74	76.26	-3908.11	7.0815	0.22325	0.11025	0.08425	5.9289	0.939429	0.835882	0.762356	18.50011	12.5712
	15_4i	61.369	281.54	78.46	-3989.25	8.67175	0.33375	0.16625	0.141	12.9818	1.037468	0.914713	0.678303	30.63714	17.6553
	15_4j	61.599	280.41	79.59	-3965.3	8.191	0.24775	0.127	0.1075	8.7624	1.008876	0.891863	0.75443	26.581	17.8186
	15_4k	60.409	276.19	83.81	-4034.3	11.7318	0.34125	0.11725	0.199125	30.8619	1.203068	1.044836	0.71635	65.02431	34.1624
	15_4l	60.656	272.26	87.74	-4938.9	32.248	1.56325	0.94525	0.54075	785.4069	1.974553	1.604578	0.208302	806.3699	20.963
	15_4m	60.588	270.31	89.69	-4357.31	18.8735	0.678	0.31225	0.358875	125.5651	1.518694	1.282784	0.553564	212.4394	86.8743
	15_4n	58.241	270.39	89.61	-4334.47	11.4528	0.451	0.296	0.137125	32.6102	1.188963	1.033898	0.620678	61.24177	28.6316
	15_4o	58.747	277.6	82.4	-4120.62	11.3628	0.394	0.21625	0.135625	31.1687	1.184375	1.030335	0.667335	60.05044	28.8817

Type	Crater ID	Latitude	W Longitude	E Longitude	Elevation	Diameter	Depth I	Depth II	Rim Height	Volume	Predicted Depth I	Predicted Depth II	Filled Fraction of Crater Depth	Predicted Volume	Fill Volume
Type I	16_1b	77.464	258.58	101.42	-4351.93	9.802	0.14175	0.00525	0.12075	9.4735	1.101658	0.965597	0.87133	41.56578	32.0923
	16_1d	76.121	269.47	90.53	-4382.52	10.8898	0.24925	0.08825	0.1105	17.5901	1.159955	1.011319	0.785121	54.01781	36.4277
	16_1f	74.961	258.25	101.75	-4340.88	13.5	0.25425	0.09075	0.140857	20.7226	1.288742	1.110705	0.802715	92.23452	71.5119
	16_2b	71.213	260.81	99.19	-4022.95	9.28225	0.1885	0.0535	0.102875	10.205	1.072637	0.942662	0.824265	36.29268	26.0877
	16_2c	70.157	256.78	103.22	-4983.15	36.1613	1.59075	0.96175	0.514125	959.1164	2.088535	1.681198	0.238342	1072.478	113.362
	16_3a	67.903	267.16	92.84	-5309.58	27.1655	2.0325	1.354	0.594125	653.0969	1.815395	1.49506	-0.11959	526.0978	126.999
	16_3e	66.411	260.27	99.73	-4143.73	15.8055	0.35925	0.0865	0.21	46.2852	1.392254	1.189005	0.741965	136.5825	90.2973
	16_3f	64.537	263.76	96.24	-4296.08	14.3818	0.51075	0.258	0.198625	55.0699	1.329322	1.141567	0.615782	107.9726	52.9027
	16_3g	63.681	249.79	110.21	-4313.95	5.57775	0.20625	0.1005	0.092125	3.7161	0.844989	0.77684	0.755914	10.32355	6.60745
	16_3i	63.856	243.97	116.03	-4372.6	9.0425	0.331	0.12575	0.1715	15.2518	1.058971	0.931822	0.687432	34.00328	18.7515
	16_3j	67.34	240	120	-4441.54	8.8735	0.35475	0.231	0.12725	15.1655	1.049226	0.924076	0.661894	32.44284	17.2773
	16_3l	67.09	246.43	113.57	-4597.55	20.2408	0.862	0.431	0.364875	182.152	1.571642	1.321457	0.451529	252.8521	70.7001
	16_3m	67.796	250.62	109.38	-4485	7.06075	0.5375	0.36375	0.120125	12.355	0.938079	0.834787	0.427021	18.36542	6.01042
	16_4a	62.429	256.61	103.39	-4409.33	12.9385	0.4345	0.2045	0.19625	40.4976	1.262193	1.090397	0.655758	82.97617	42.4786
	16_4b	61.838	268.65	91.35	-2119.71	6.09925	0.314	0.168	0.119375	5.0174	0.908434	0.83837	0.65435	13.27107	8.25367
	16_4c	61.657	267.34	92.66	-4109.99	5.80175	0.14875	0.02075	0.111675	2.9425	0.872373	0.803386	0.829488	11.53135	8.58885
	16_4d	60.427	262.44	97.56	-4301.88	8.754	0.2615	0.11475	0.128375	13.7884	1.042278	0.918546	0.749107	31.36582	17.5774
	16_4g	58.848	267.74	92.26	-4191.41	5.34225	0.18025	0.07025	0.09725	2.9576	0.815973	0.748729	0.779098	9.14501	6.18741
	16_4h	57.799	266.38	93.62	-4330.74	5.8085	0.2045	0.08325	0.106	4.113	0.873195	0.804184	0.765803	11.56908	7.45608
	16_4i	59.074	264.53	95.47	-4458.79	9.283	0.4205	0.25875	0.10825	22.5504	1.072679	0.942696	0.607991	36.29998	13.7496
	16_4j	59.758	256.85	103.15	-4284.02	8.73925	0.2635	0.07175	0.14775	8.576	1.041417	0.91786	0.746979	31.23439	22.6584
	16_4k	58.677	247.57	112.43	-4531.49	9.3075	0.242	0.08675	0.14825	12.3178	1.074065	0.943794	0.774688	36.539	24.2212
	16_4l	58.532	243.17	116.83	-4812.99	16.948	0.587	0.33	0.193875	81.3074	1.44069	1.225169	0.592556	162.5052	81.1978
	16_4m	60.391	244.14	115.86	-4658.74	15.8488	0.47175	0.28025	0.187625	62.9191	1.39412	1.190403	0.661614	137.515	74.5959
	16_4q	60.964	253.1	106.9	-4363.56	5.10475	0.13675	0.038	0.08325	2.1677	0.786464	0.720161	0.82612	8.047991	5.88029
	14_3n	64.912	9.1497	350.8503	-6609.51	130.102	2.56	1.65825	0.89875	20717.33	3.911117	3.25167	0.345456	25997.13	5279.79
Type II	7_2f	72.772	195.43	164.57	-5976.34	81.98	2.36075	1.36475	0.79975	6372.427	3.119029	2.308918	0.243114	8231.805	1859.38
	9_1a	77.182	145.68	214.32	-5853.3	52.3713	1.917	1.02475	0.73025	1947.329	2.504137	1.948145	0.234467	2697.142	749.813
	12_1h	74.256	40.814	319.186	-5416.21	17.0273	0.4885	0.2625	0.204375	56.0839	1.443987	1.22762	0.661701	164.4039	108.32
	12_2a	71.193	50.98	309.02	-5372.86	18.8983	0.38525	0.26575	0.11525	55.164	1.519669	1.2835	0.746491	213.1337	157.97
	16_1c	77.115	270.9	89.1	-4471.39	31.0938	0.7425	0.12125	0.56725	311.9858	1.939601	1.580782	0.617189	736.4079	424.422
Type III	1_4d	79.125	299.09	60.91	-5096.19	24.4463	1.12075	0.62775	0.30775	260.394	1.723957	1.430781	0.349897	404.586	144.192
	2_2a	81.582	169.88	190.12	-4814.89	18.8738	1.025	0.67275	0.206875	161.7666	1.518704	1.282791	0.325082	212.4464	50.6798
	2_4a	81.264	105.17	254.83	-4857.47	18.2415	0.6595	0.522	0.081125	86.6483	1.493558	1.264302	0.558437	195.1655	108.517
	3_3d	78.606	13.005	346.995	-5035.34	12.756	0.30775	0.10975	0.14625	21.8952	1.253437	1.083679	0.754475	80.09244	58.1972
	4_2a	81.101	271.17	88.83	-4434.37	8.67825	0.16425	0.03125	0.08075	7.3643	1.037849	0.915017	0.84174	30.69435	23.3301
	4_2c	81.36	242.75	117.25	-4574.84	11.0595	0.1485	0.05625	0.074125	7.5194	1.16878	1.0182	0.872944	56.13888	48.6195
	14_1a	78.598	28.233	331.767	-5592.42	20.3373	0.8925	0.5525	0.249875	125.199	1.575309	1.324123	0.433444	255.8645	130.665

Appendix B: Gridview Instructions

In addition to viewing the grids, Gridview has several tools found in the "Tools" menu which help to analyze the data (Figure 1).

Figure 1:

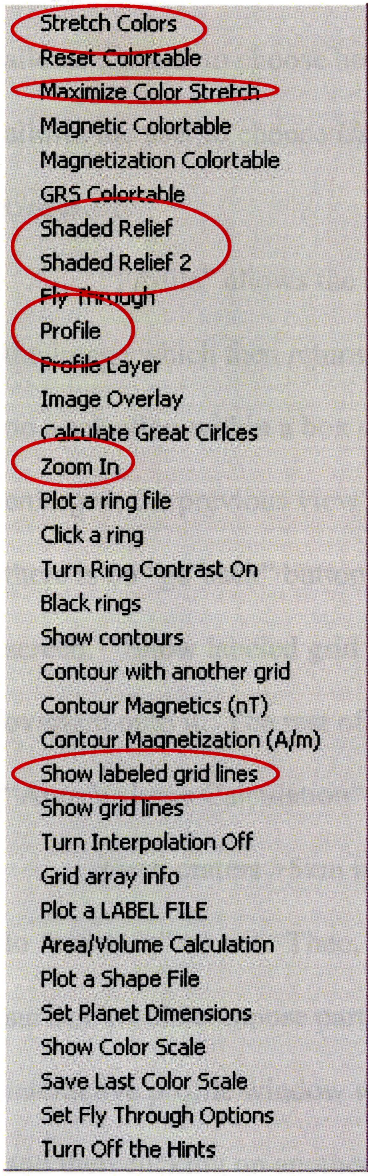

S

"Maximize Color Stretch" simply maximizes the range of colors in the image so that cool colors represent the lower elevation areas, warm colors represent the higher elevation areas, and black and white represent the deepest and highest areas respectively. "Stretch Colors" allows the user to stretch the colors of the image by hand. "Shaded Relief" and "Shaded Relief 2" return a shaded relief image; both selections produce a window for the user to input options for light angle (deg), light azimuth (deg), and exaggeration. The difference between these two options is that "Shaded Relief" only allows the user to choose between a grayscale or color Image while "Shaded Relief 2" allows the user to choose *Use the current color stretch*, *Maximum color stretch*, or *Grayscale.*

"Profile" allows the user to create a topographic profile by clicking two points on the image which then returns a generated profile discussed later. "Zoom In" will zoom in on a selection within a box drawn by the user. As soon as a section of the image has been enlarged, the previous view is deleted due to the large file size of each image; as a result, there is no "go back" button and to get to a different view, one must refresh the entire screen. "Show labeled grid lines" returns the same image, but with labeled gridlines overlain onto it. The rest of the options were not used with the exception of "Area/Volume Calculation" which will be discussed later.

First, craters >5km in diameter were visually identified and the program was used to "zoom-in" on a it. Then, a profile was drawn across the crater so that the pre-impact surface would compose part of each side of the profile (Figure 2). Gridview returns an interactive profile window where measurements may be taken by clicking on one point and then clicking on another; to draw a vertical or horizontal line, the shift-key must be held down. If the line drawn was completely vertical or horizontal, Gridview gives a distance output (Figure 3, point A). If the line was drawn at an angle, Gridview will give a slope output (Figure 3, point B). In this window, several measurements are taken including the following which are then indicated in Figure 6.

Figure 2:

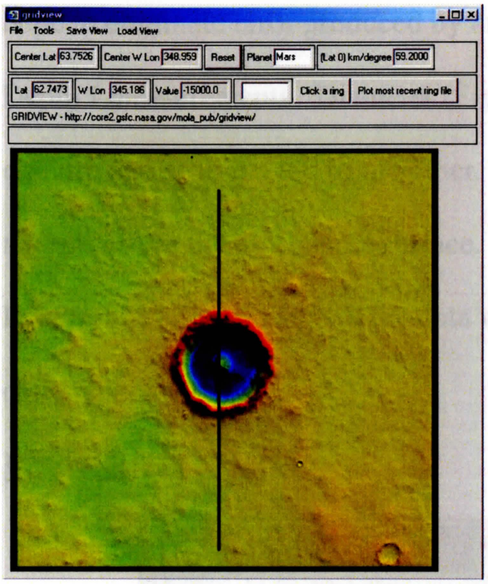

Figure 3:

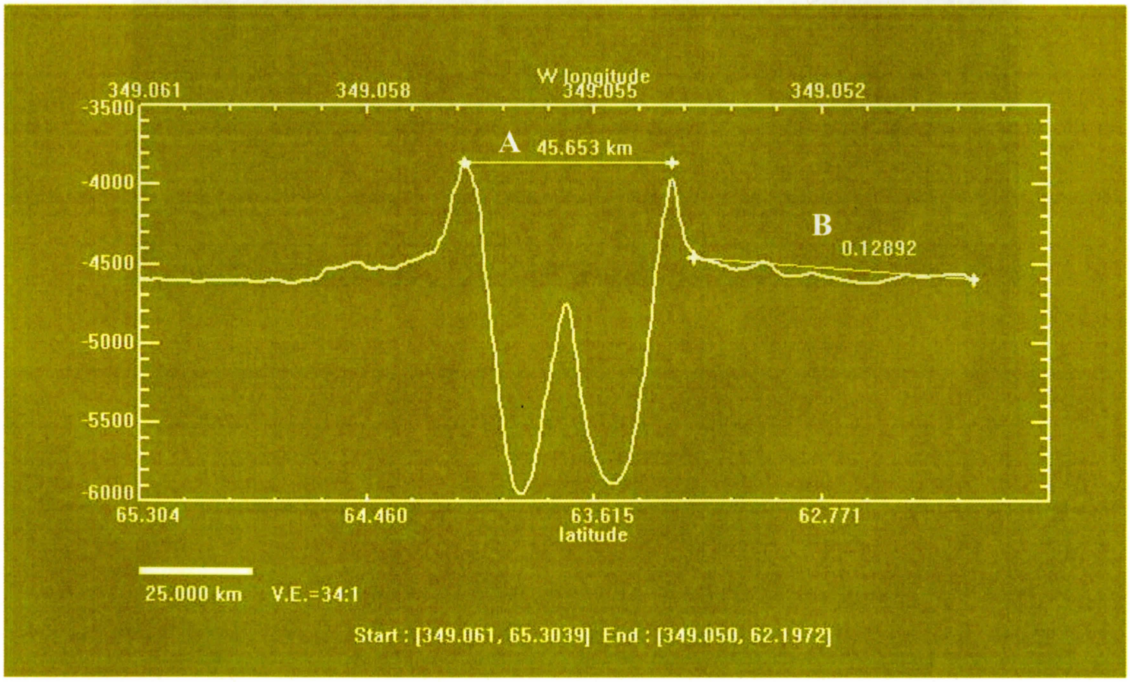

The Depth I measurement (Figure 4a) is the measurement between the top of the rim and the bottom of the crater. This measurement coincides with the depth measurements gathered by Garvin et al. The crater depth measured from the pre-impact surface, Depth II (Figure 4b), was also gathered. By gathering this measurement, we hope to eliminate error produced by eroding of the rim which could be encountered with Depth I measurements. Diameter (Figure 4c) is simply the measurement from the top of one rim across to the top of the other. Rim height (Figure 4d) is the height of the top of the rim above the pre-impact surface. For each crater, four profiles were taken (N-S, W-E, NW-SE, NE-SW) and all the data were averaged to achieve a single value for each crater characteristic.

Figure 4:

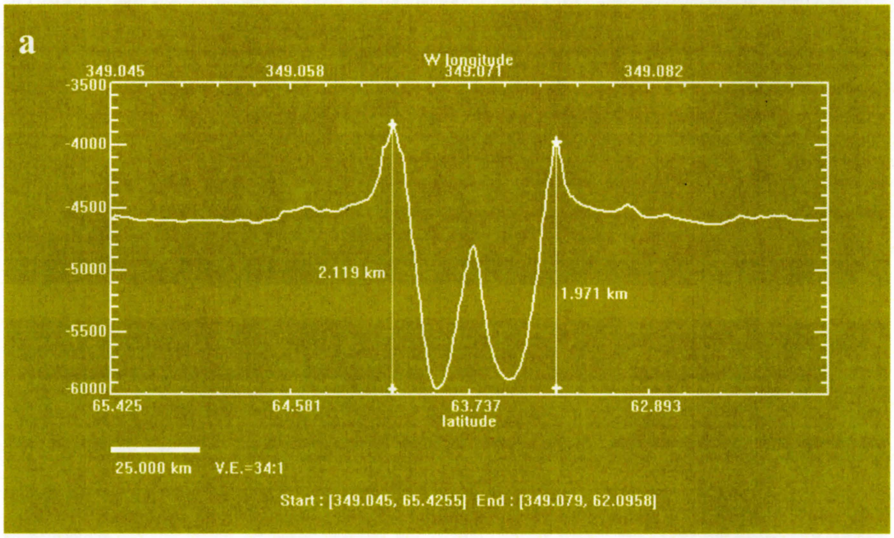

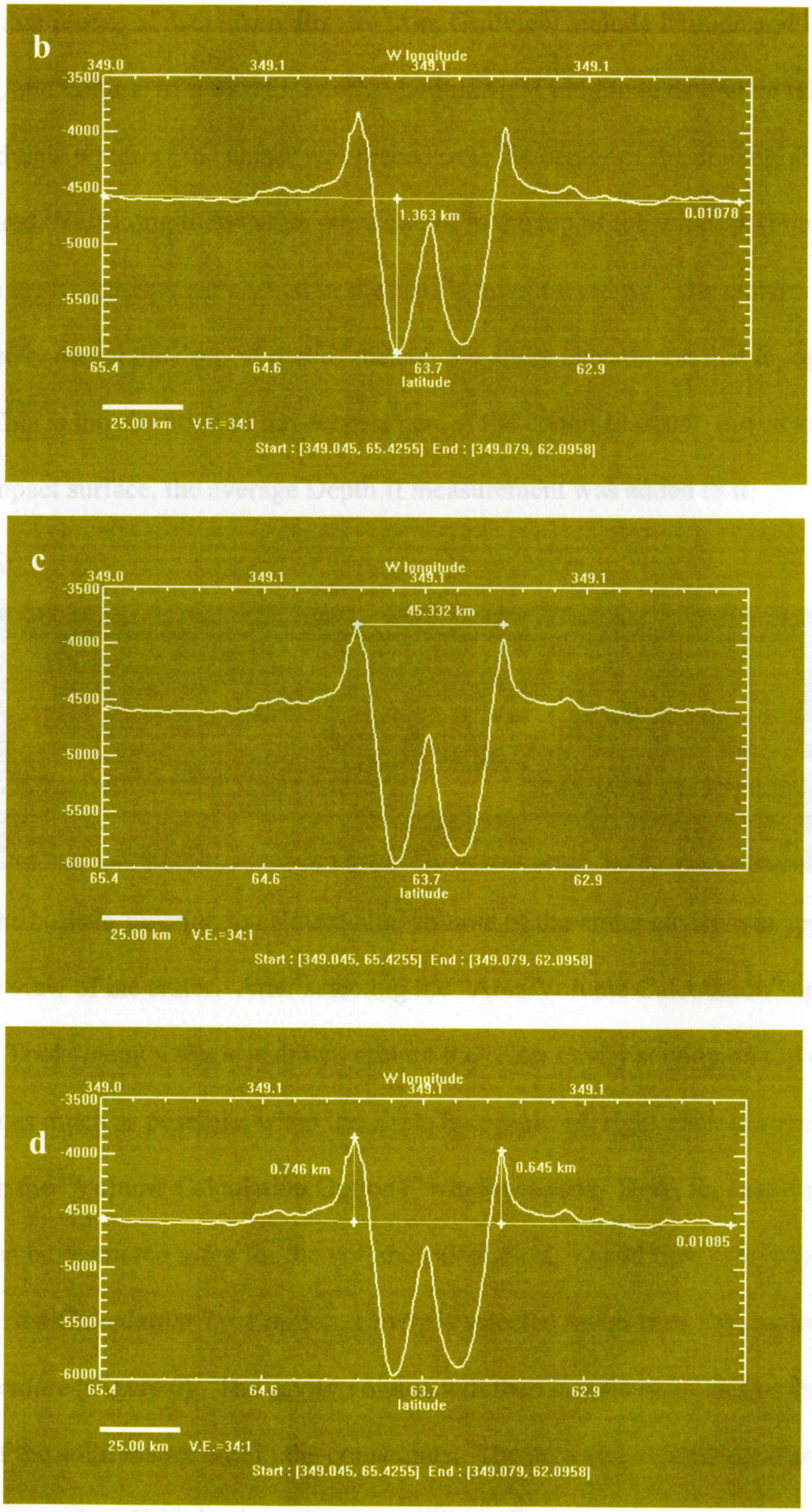
b
W longitude
349.0
349.1
349.1
349.1
-3500
-4000
-4500
-5000
-5500
-6000
1.363 km
0.01078
65.4
64.6
63.7
62.9
latitude
25.00 km
V.E.=34:1
Start : [349.045, 65.4255] End : [349.079, 62.0958]
c
W longitude
349.0
349.1
349.1
349.1
-3500
-4000
-4500
-5000
-5500
-6000
45.332 km
65.4
64.6
63.7
62.9
latitude
25.00 km
V.E.=34:1
Start : [349.045, 65.4255] End : [349.079, 62.0958]
d
W longitude
349.0
349.1
349.1
349.1
-3500
-4000
-4500
-5000
-5500
-6000
0.746 km
0.645 km
0.01085
65.4
64.6
63.7
62.9
latitude
25.00 km
V.E.=34:1
Start : [349.045, 65.4255] End : [349.079, 62.0958]

Other pieces of data taken directly from Gridview include latitude and longitude, elevation, and volume of the crater cavity. Latitude and longitude data were taken in the main Gridview window; the curser was placed over the center of the crater and the Latitude and West Longitude values were output in the top of the window (Figure 5). Elevation measurements were taken in the profile output window. The cursor is placed on or directly above the deepest part of the crater and the elevation at that topography is output. This is the elevation of the deepest part of the crater; to obtain the elevation of the pre-impact surface, the average Depth II measurement was added to it.

<u>Figure 5:</u>

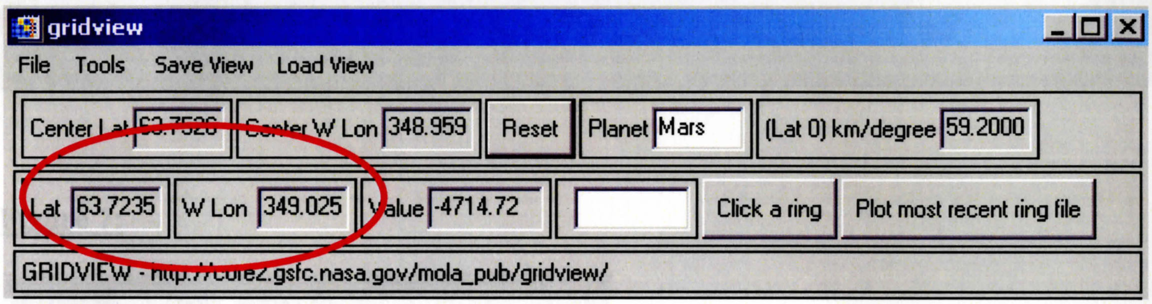

The built-in function to calculate the volume of the crater cavity was applied from a zoomed view of the crater. After selecting the "Area/Volume Calculation" option under the Tools-menu a shape is drawn around the crater cavity staying on top of the crater rim as much as possible; when the circle is completed, right click to save the shape file. Then the "Volume Calculation Options" window opens. Here, the crater profile images can be restricted more for the volume calculation. In addition, it is imperative that under the *Calculation Type* option, *Cavity* is selected rather than *Volume* and then press *Calculate* (Figure 6). The <u>cavity</u> volume will then be calculated rather than the volume of the solid matter within the constraints. The area and volume measurements are then returned on Gridview's main screen (Figure 7).

Figure 6:

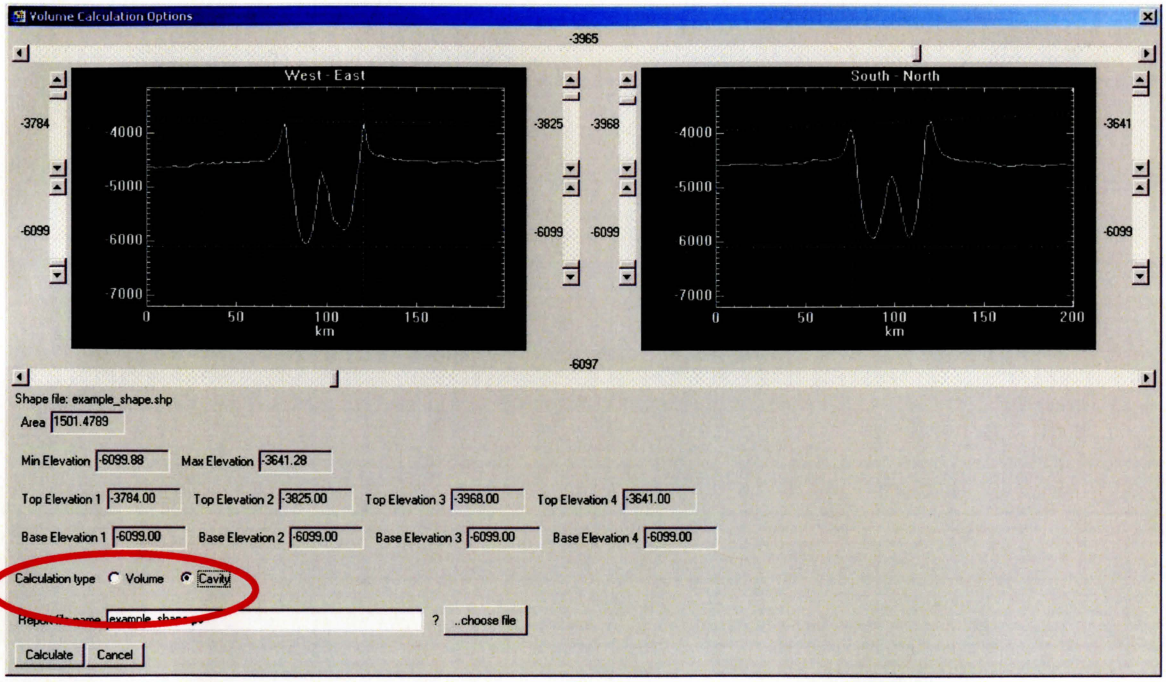

Figure 7: